

N73-26438

REMOTE MONITORING OF SOIL MOISTURE USING AIRBORNE MICROWAVE RADIOMETERS

by

C. L. Kroll

June 1973

**CASE FILE
COPY**

supported by

National Aeronautics and Space Administration
NASA Grant NGL 44-001-001
NASA Contract NAS 9-11155



TEXAS A&M UNIVERSITY
REMOTE SENSING CENTER
COLLEGE STATION, TEXAS



REMOTE MONITORING OF SOIL MOISTURE
USING AIRBORNE MICROWAVE RADIOMETERS

by

C. L. Kroll

June 1973

supported by

National Aeronautics and Space Administration

NASA Grant NGL 44-001-001

NASA Contract NAS 9-11155

ABSTRACT

Several remote sensors have been proposed as potentially applicable for monitoring soil moisture. Microwave sensors appear to have an advantage over shorter wavelength sensors because of their deeper penetration into the soil and their relative immunity to atmospheric effects. The capability of airborne microwave radiometers to monitor soil moisture was investigated.

In this report the current status of microwave radiometry is provided. The fundamentals of the microwave radiometer are reviewed with particular reference to airborne operations, and the interpretative procedures normally used for the modeling of the apparent temperature are presented.

Airborne microwave radiometer measurements were made over selected flight lines in Chickasha, Oklahoma and Weslaco, Texas. Extensive ground measurements of soil moisture were made in support of the aircraft mission over the two locations. In addition, laboratory determination of the complex permittivities of soil samples taken from the flight lines were made with varying moisture contents.

The data were analyzed to determine the degree of correlation between measured apparent temperatures and soil moisture content. The Chickasha fields were fairly dry

(<20° moisture content) and no correlation of apparent temperature with soil moisture existed for the Chickasha data. A heavy rain preceding the Weslaco flight invalidated the ground soil moisture measurements. However, an assumed value of the soil moisture content of the Weslaco fields was derived from known moisture retention curves for the soil type. The combined results of the Chickasha and Weslaco experiments using the derived soil moisture value yielded a high degree of correlation of apparent temperature and soil moisture. Regression analysis indicated a $-2.15^{\circ}\text{C}/\text{percent}$ moisture variation in apparent temperature for the 1.42 GHz radiometer, vertical polarization, for bare or nearly bare fields, which compares favorably with the results reported by Jean [10]. The center cell of the 19.4 GHz, horizontal, polarization, had an average variation in apparent temperature of $-1.5^{\circ}\text{C}/\text{percent}$ moisture when observing vegetated fields.

ACKNOWLEDGEMENTS

Sincere thanks are extended to Mr. Bruce J. Blanchard of the USDA Southern Plains Watershed Research Center, Chickasha, Oklahoma for the ground support measurements and for many helpful conversations. I also wish to thank Dr. Craig Wiegand, Mr. Alvin Gerbermann, and Mr. Joe Cuellar of the USDA Rio Grande Soil and Water Research Center, Weslaco, Texas, for their assistance in the ground support measurements. The cooperation of the NASA Goddard Space Flight Center and Dr. Thomas Schmutge in conducting the airborne microwave radiometer mission is gratefully acknowledged.

I would like to express special appreciation to my many colleagues and associates of the Remote Sensing Center, Texas A&M University, particularly Mr. Terry Sibley and Mr. Bill Lee for their help in the dielectric measurements and the data reduction.

The financial support of this research was provided by the National Aeronautics and Space Administration under NASA Grant NGL 44-001-001 and NASA Contract NAS 9-11155.

TABLE OF CONTENTS

<u>Chapter</u>	<u>Page</u>
I. INTRODUCTION	1
The Microwave Radiometer as a Remote Sensor	3
Value of Remotely Sensing Soil Moisture	7
Objectives	9
Scope of This Report	10
II. PRINCIPLES OF MICROWAVE RADIOMETRY	12
Thermal Emission	12
Sensor Operation	16
III. INTERPRETATION OF RADIOMETRIC DATA	26
The Concept of Apparent Temperature	26
Models	29
Surface Roughness and Vegetation Effects	31
Application to Soil Moisture Detection	33
IV. SOILS AS DIELECTRICS	41
Introduction to Soil Systems	42
Measurement of the Complex Dielectric Constant	50
V. AIRBORNE MEASUREMENTS PROGRAM	65
Description of Test Sites	65
Chickasha	65
Weslaco	75
Aircraft Program	78

<u>Chapter</u>	<u>Page</u>
Results of the Flights	80
Summary of Airborne Experiment	82
VI. ANALYSIS OF EXPERIMENTAL DATA	84
Chickasha Data Analysis	85
Weslaco Data	92
Combined Analysis of Chickasha and Weslaco Data	94
Summary of Data Analysis	99
VII. CONCLUSIONS AND RECOMMENDATIONS	101
REFERENCES	104
APPENDIX A	109

LIST OF TABLES

<u>Table</u>		<u>Page</u>
IV-I	Classification of Soil Moisture	49
V-I	Radiometer Systems on Board the NASA CV-990 Aircraft March 14, 1972	79
VI-I	Correlation of Apparent Temperature and Soil Moisture Content	98
A-I	Chickasha Apparent Temperatures	110
A-II	Weslaco Apparent Temperatures	115
A-III	Soil Moisture Survey, Chickasha Sites . . .	126
A-IV	Wheat Samples from Chickasha Sites	127

LIST OF FIGURES

<u>Figure</u>		<u>Page</u>
II-1	System diagram for a typical Dicke radiometer	18
III-1	Relative complex dielectric constant for sand versus moisture content	35
III-2	Emissivity as a function of look angle	37
III-3	Emissivity as a function of moisture content	38
IV-1	USDA fractionation of soil particles	43
IV-2	Soil textural triangle	45
IV-3	Specific surface versus particle diameter [36]	46
IV-4	Waveguide measurement system for determining complex dielectric constant	57
IV-5	Relative complex dielectric constant for all soils tested	61
IV-6	Relative complex constant for silty loam and loamy soils	62
IV-7	Relative complex dielectric constant for all silty clay loams	63
IV-8	Relative complex dielectric constant for a fine sandy loam	64
V-1	Chickasha test sites: (a) site A (b) site B	67
V-2	Chickasha test sites: (a) site G (b) site H	68
V-3	Chickasha test site I	69
V-4	Ground cover for Chickasha sites: (a) site A (b) site B	71

<u>Figure</u>		<u>Page</u>
V-5	Ground cover for Chickasha sites: (a) site C (b) site F	72
V-6	Ground cover for Chickasha sites: (a) site G (b) site H	73
V-7	Distribution of percent moisture for Chickasha soil samples	74
V-8	Distribution of percent moisture for Weslaco soil samples	76
V-9	Typical fields along Weslaco flight line	77
VI-1	1.42 GHz radiometer results for sites I, J and K	86
VI-2	1.42 GHz radiometer results for Chickasha test sites	87
VI-3	19.4 GHz radiometer results for Chickasha test sites	88
VI-4	37.0 GHz radiometer results for Chickasha test sites	89
VI-5	Apparent temperatures versus wheat mois- ture for Chickasha test sites	90
VI-6	Photomosaic of a portion of the Weslaco flight line with corresponding apparent temperatures	93
VI-7	Combined results of the 1.42 GHz radio- meter, vertical polarization	95
VI-8	Combined results of the 1.42 GHz radio- meter, horizontal polarization	96

CHAPTER I

INTRODUCTION

The remote sensing community has several sensors at its disposal, however, few sensors offer as great a potential as those operating in the microwave portion of the electromagnetic spectrum. The microwave region sensors have several features which qualify them a position among operational remote sensors such as aerial photography and infrared imaging systems. Sensors operating at microwave wavelengths are not restricted to daylight operation, and the weather limitations, so critical to the infrared and visible wavelength sensors, are far less restrictive. Some microwave wavelengths are susceptible to atmospheric effects (e.g. 22.235 and 60 GHz, absorption lines for water vapor and molecular oxygen, respectively) thus microwave sensors can be used in monitoring atmospheric phenomena. In observing terrestrial objects with visible wavelengths, little information is directly obtained except from the very near surface, whereas the longer microwave wavelengths penetrate below the surface, hence some knowledge of the sub-surface is contained in

The citations on the following pages follow the style of the Proceedings of IEEE.

the total information content of data from microwave sensors.

Microwave sensors fall into two categories: active and passive. The active microwave sensor is radar. Radar remote sensors are used in a stationary position or from moving platforms, either aircraft or satellite. For remote sensing applications, stationary positioned radars are used in observing atmospheric phenomena, whereas airborne radars are most often used to observe terrestrial areas and the oceans. The side looking airborne radar (SLAR) and the radar scatterometer are two prominent airborne radars used in earth observations. Both sensors are used in aircraft operations, and a scatterometer system is included in the package of sensors aboard the Skylab orbiting platform.

In the same package of sensors slated for the Skylab program will be the lesser known of the microwave sensors, the microwave radiometer. Used to measure the natural microwave emissions of an object, the radiometer can be designed for use as either a scanning device or a fixed look angle device. The fixed look angle design is being used in some satellite observations, aircraft operations, and for work in the field, usually from a truck mounted platform. A scanning radiometer is presently used in a NASA aircraft.

The Microwave Radiometer as a Remote Sensor

Of particular attention in this thesis is the passive microwave sensor, the radiometer. The radiometer measures the natural radiation of an object within a specified band of frequencies. This natural radiation is commonly referred to as thermal noise. Any object emits radiation according to its absolute temperature and inherent emission characteristics. If two objects have the same physical temperature and differ in emission characteristics, then, assuming the emissions of both objects can be measured, the two are distinguishable.

Natural radiation at microwave wavelengths is weak, thus high gain amplifiers are a requirement in the design of radiometers. High gain amplifiers are plagued by inherent gain fluctuations, and not until the radiometer design proposed by Dicke in 1946 [1] has a means of accurately discerning emission characteristics at microwave frequencies been possible.

During the past decade the scientific community has proposed many uses for the microwave radiometer. Oceanographic applications of the radiometer have been investigated for determining sea state [2], surface temperatures of the ocean [3], and surface salinity [4].

Sea state measurements were made by Hollinger [2] from a tower on Argus Island, using radiometers at 1.41, 8.36 and 19.34 GHz. His data indicate a frequency dependent correlation between apparent temperatures and wind speeds from calm winds to 15 meters per second velocities. Apparent temperatures increased with increasing surface roughness and foaming. Paris [4] studied the dielectric properties of sea water as they are affected by salinity. He found that from 1-3 GHz the effect of salinity on microwave emissions is significant, but for frequencies above 4 GHz salinity effects can be neglected.

In another study, Paris [5] examined the general problem of thermal radiation in the atmosphere at microwave frequencies. The direct problem of radiative transfer is solved for plane-parallel, homogeneous, model atmospheres from derived regression equations for the volume absorption coefficient of rain and known expressions for those of clouds, molecular oxygen, and water vapors. In addition, the effect of multiple scattering on the transfer of thermal microwaves in the atmosphere is evaluated at 37 GHz by the Monte Carlo method for a model cloud. From his studies, Paris concludes that a radiometer operating at 10.69 GHz can be used to survey the integrated content of liquid water in the rain mass

over the ocean; a set of radiometers operating at 5.81, 10.69, 15.375 and 19.35 GHz may be used to survey sea state, atmospheric liquid water, and precipitable water over the ocean; and a radiometer operating at 37 GHz can be used to detect hail and heavy rain over land; however, a microwave radiometer cannot be used to survey sea temperature.

Weger [6] derived expressions for calculating apparent sky temperatures for a variety of weather conditions, and Edison [7] calculated the contribution of water and ice clouds to zenith sky temperatures in the frequency range from 10 to 100 GHz. The Nimbus E satellite has a set of five radiometers operating at 21.2, 31.4, 53.65, 54.9 and 58.8 GHz. With the two lower frequency radiometers operating near the water vapor absorption line and the three higher radiometers near the line for oxygen, the combined information is predicted to show many climatic conditions undetectable using infrared or visible wavelength sensors [8].

Aukland and Conway [9] report that an oil layer on a rough sea produced a decrease in measured apparent temperatures due to the calming effect of the oil film. Jean [10] reports that an oil film on a water surface does produce an apparent temperature anomaly, but no functional relationship between oil film thickness and

apparent temperature could be determined from his data.

Gloersen, et al. [11] show vivid qualitative results of a scanning radiometer operating at 19.35 GHz distinguishing between new and old Arctic ice.

In addition to the oceanographic and meteorological application of microwave radiometry, recently many investigators have addressed the question of detecting soil moisture content. The dielectric properties of the soil are strongly affected by moisture content. In turn, the emission characteristics of an object are dependent on the dielectric properties of the object. Kennedy and Edgerton [12] first proposed the concept of monitoring soil moisture content, and they demonstrated that apparent temperatures are effected by moisture content. They also suggest that measuring soil moisture as a function of depth is possible. Mason [13] reports that from an airborne radiometer measurements at 1 to 2 cm wavelengths, a moist layer of soil more than 0.1 inch below a dry surface layer could not be detected. Jean [10] feels that perhaps neither extreme is altogether correct, and in particular points to Basharinov and Skutko [14] who were able to infer moisture contents to within a 3% moisture content value from measurements of a 10 cm wavelength radiometer.

More recent investigators have included Richerson

[15], Jean [10], Jean et al. [16], Poe et al. [17], and Schmugge et al. [18]. Richerson [15] reports a change of 1.5 and 1.6 °K for each one percent moisture variation using a tower based radiometer operating at 31.4 GHz for the vertical and horizontal polarizations, respectively. Jean et al. [16] and Jean [10] report the results of an airborne experiment using radiometers operating at 1.42, 2.69, 4.99, and 10.69 GHz. Their results were encouraging, however, only a limited amount of data was obtained from the experiment.

In reviewing the past studies in radiometric application, certain limitations which hinder their development become apparent: 1) spatial resolution and antenna efficiency are critical, especially with the longer wavelength radiometers, 2) system sensitivity, 3) antenna size and weight limitations for remote platform operation, and 4) the large number of unknown parameters make interpretation difficult.

Value of Remotely Sensing Soil Moisture

A remote sensor capable of monitoring soil moisture content could be applied in the disciplines of hydrology and agriculture. The hydrologist has a need for a soil moisture monitoring capability. A thorough hydrologic analysis of data for a watershed study required the

development and use of mathematical models to adequately describe the movement of water from the time it falls on the ground as rain until it is absorbed by the soil, evaporates, used by the plants, or discharged in rivers and streams [19]. A basic element in any watershed model is to distinguish between the water which is stored in the soil surface and the quantity of surface runoff. A good index of this element is the surface soil moisture condition. At present, no adequate method of monitoring this surface soil moisture exists because of the large areas which need to be observed [19]. Airborne microwave radiometers show promise in providing the desired index.

The agriculture community could employ remote sensing techniques to help evaluate the timely irrigation of crops, especially on the larger commercial farms. Planting and tilling operations have optimum levels of moisture content in order to be most effective, and a remote monitor of soil moisture may find application for such farm management procedures.

In addition to the use of microwave radiometry, several other remote sensors have been investigated for the possible detection of soil moisture content in soils. Radar scatterometers, infrared photography, and various experiments with optical frequencies are under investigation. Infrared imagery can qualitatively identify very

moist fields. A photopolarimeter [20] has been shown to measure the difference in polarizations of reflected sunlight for moist and dry fields, however, only the very thin surface layer is observed, thereby reducing the systems effectiveness in an arid region where the soil normally has a dry, crusty surface regardless of the actual moisture content below the top few centimeters.

Rouse [21] has introduced the possibility of using radar scatterometers to measure soil moisture content, and Moore et al. [22] have provided some experimental results which show some dependence of radar cross sections to moisture content. Multispectral photography was used by Werner and Schmer [23] to investigate moisture detection capabilities, and reasonable qualitative results appear feasible.

Objectives

The primary objective of the research effort reported here was to examine the specific application of determining soil moisture content using airborne microwave radiometers. Three main areas of work were established:

- 1) laboratory measurement of the complex permittivities of soil with varying moisture contents,
- 2) airborne radiometer flights over selected test

sites with accompanying ground measurements of soil moisture in each site, and

- 3) analysis of the results of the experimental phases and an examination of appropriate theoretical models for passive microwave remote sensing.

Scope of This Report

This report describes the experimental advancement of the application of microwave radiometry to monitor soil moisture content.

Chapter II and III provide an understanding of radiometric principles and the basis for interpretation. The process of thermal emission at microwave frequencies is discussed, and basic radiometer sensor operation is reviewed. The concept of apparent temperature and various theoretically modeling approaches are presented.

Chapter IV deals with the soils and their dielectric properties. A brief introduction to soil-water systems is given, followed by the basis and procedure for the measurement of the complex permittivities. Pertinent results of the measurements are also presented.

Chapter V describes the airborne phase of the experiments. A description of the two test sites in Weslaco, Texas and Chickasha, Oklahoma are given, along with

an account of the ground observations. The aircraft program is presented and an overall discussion of the results is provided.

Chapter VI is concerned with the analysis of experimental data. The methods used for the analysis are discussed and the results of the analysis are reported with comparisons to previous investigations. Chapter VII gives conclusions and recommendations for further study.

CHAPTER II

PRINCIPLES OF MICROWAVE RADIOMETRY

Thermal Emission

The fundamental physical basis for passive microwave sensing is that everything which has temperature above absolute zero emits radiation. In analytical form, the radiation intensity from a perfect blackbody is given by Planck's radiation law [24]

$$K = \frac{hf^3}{c^2} \left[\frac{1}{\exp(hf/kT) - 1} \right] \text{ j/m} \quad (\text{II-1})$$

where: h = Planck's constant

h = 6.626×10^{-34} joule-seconds

c = speed of light

c = 3×10^8 meters/second

k = Boltzman's constant

k = 1.38×10^{-23} joules/°K

f = frequency of radiation

T = absolute temperature

In the microwave region of the spectrum (II-1) may be expressed by the Rayleigh-Jeans approximation. By expanding the exponential term in (II-1) and neglecting higher order terms

$$K = \frac{hf^3}{c^2} \left[\frac{1}{1 + \frac{hf}{kT} + \dots - 1} \right] j/m \quad (\text{II-2})$$

and simplifying (II-2) gives

$$K \approx \frac{kT}{\lambda^2} j/m \quad (\text{II-3})$$

where the wavelength, λ , is used in place of the frequency. In order to change (II-3) to a measurable expression, consider the power density within a small frequency interval Δf passing through a unit solid angle. The power is given as

$$P \approx \frac{kT \Delta f}{\lambda^2} \quad (\text{II-4})$$

The power given by (II-4) is the radiated power of the blackbody. The power received by an ideal antenna, with maximum effective aperture A_{me} and uniform beamwidth Ω_{ant} directed entirely at the blackbody, is

$$P_{ant} = P A_{me} \Omega_{ant} \quad \text{watts} \quad (\text{II-5})$$

where: $A_{me} = (\lambda^2/4\pi) G_m$

$$\Omega_{ant} = 4\pi/G_m$$

$G_m =$ antenna maximum gain

Substituting (II-4) in (II-5) and simplifying gives

$$P_{ant} = k T \Delta f \quad \text{watts} \quad (\text{II-6})$$

The power received by the ideal antenna is directly proportional to the absolute temperature of the blackbody, however, no real-world objects exhibit blackbody radiation properties.

Radiation from real-world objects (non-ideal radiators) is dependent on their intrinsic electromagnetic properties. These intrinsic properties change as the physical properties of the medium change, i.e. density, internal structure, temperature, phase (solid, liquid, or gas). In addition to internal characteristics, radiation which is collected by the receiving antenna of a radiometer is strongly affected by the surface interface between the object and any intervening medium. This

interface is a product of the surface configuration, as well as the electromagnetic properties of the two media.

In order to account for non-ideal radiation, a term called emissivity is normally used. Strictly speaking, the emissivity is the intrinsic radiating capacity of an object in comparison with a blackbody, or the ratio of the power radiated by the object and the power radiated by a perfect blackbody at the same absolute temperature [24]. In microwave radiometry, the term emissivity is often used to encompass the radiation effects of the surface interface, in addition to intrinsic radiation. For purposes of this paper the emissivity will be defined to account for both inherent emission characteristics, surface interface effects, and receiver parameters peculiar to a single mode of operation, thus the emissivity, ϵ , is given by

$$\mathcal{E} = T_t / T_{bb} \quad (\text{II-7})$$

where: T_t = Radiation of target

T_{bb} = Radiation of blackbody at the same absolute temperature

and (II-6) becomes

$$P_{ant} = k T_t \Delta f = k \epsilon T_{bb} \Delta f \quad (\text{II-8})$$

where ϵ is a function of electromagnetic properties of the medium (the complex permittivity), the frequency of radiation, the polarization of the antenna, look angle, and surface roughness and vegetation. T_a corresponds to the radiated power of the object under observation and is said to be its "apparent temperature."

Sensor Operation

A radiometer is essentially a very high gain receiver which measures the thermal noise an object emits. The first radiometers were directed at stellar objects and were known as radio telescopes. The gain fluctuations of these radio telescopes were far too extreme for any type of absolute measurements, and thus application of radiometers for earth observations was nonexistent.

In 1946 Dicke [1] proposed a receiver design which reduced the large gain variations of early radiometers, thus leading to absolute temperature measurements. The unique characteristics of the Dicke radiometer (see Figure II-1) is that the receiver is alternately connected to the antenna port and a reference noise source by means of a ferrite device known as a Dicke switch. The switching operation produces a square wave modulated signal whose amplitude is proportional to the difference in the two inputs. The signal then passes through the

optional RF stages of amplification to the mixer where it is heterodyned and passed to the IF stages of amplification. The carrier frequency is removed from the signal, and a synchronous detector converts the amplitude of the square wave to a DC voltage which is proportional to the difference of the antenna and base load temperatures. The integrator provides a low pass filter to smooth the signal into the proper analog form for processing and recording.

Calibration of the Dicke radiometer is accomplished in various ways. Normally the radiometer is designed with one or more stable internal noise sources at different temperatures in addition to the base load. By proper switching, the internal calibration source replaces the antenna load in the system, and the output is calibrated to correspond to the difference in noise source temperatures. Additional switching will compare the base noise source to itself, providing the correct zero offset voltage for the analog output. Since all elements in the system have an inherent noise and insertion loss, in order to calibrate the radiometer for absolute temperatures, an external calibration source must be utilized. This is accomplished by a material which approximates blackbody radiation for the frequency of interest placed directly in front of the antenna. Coupled

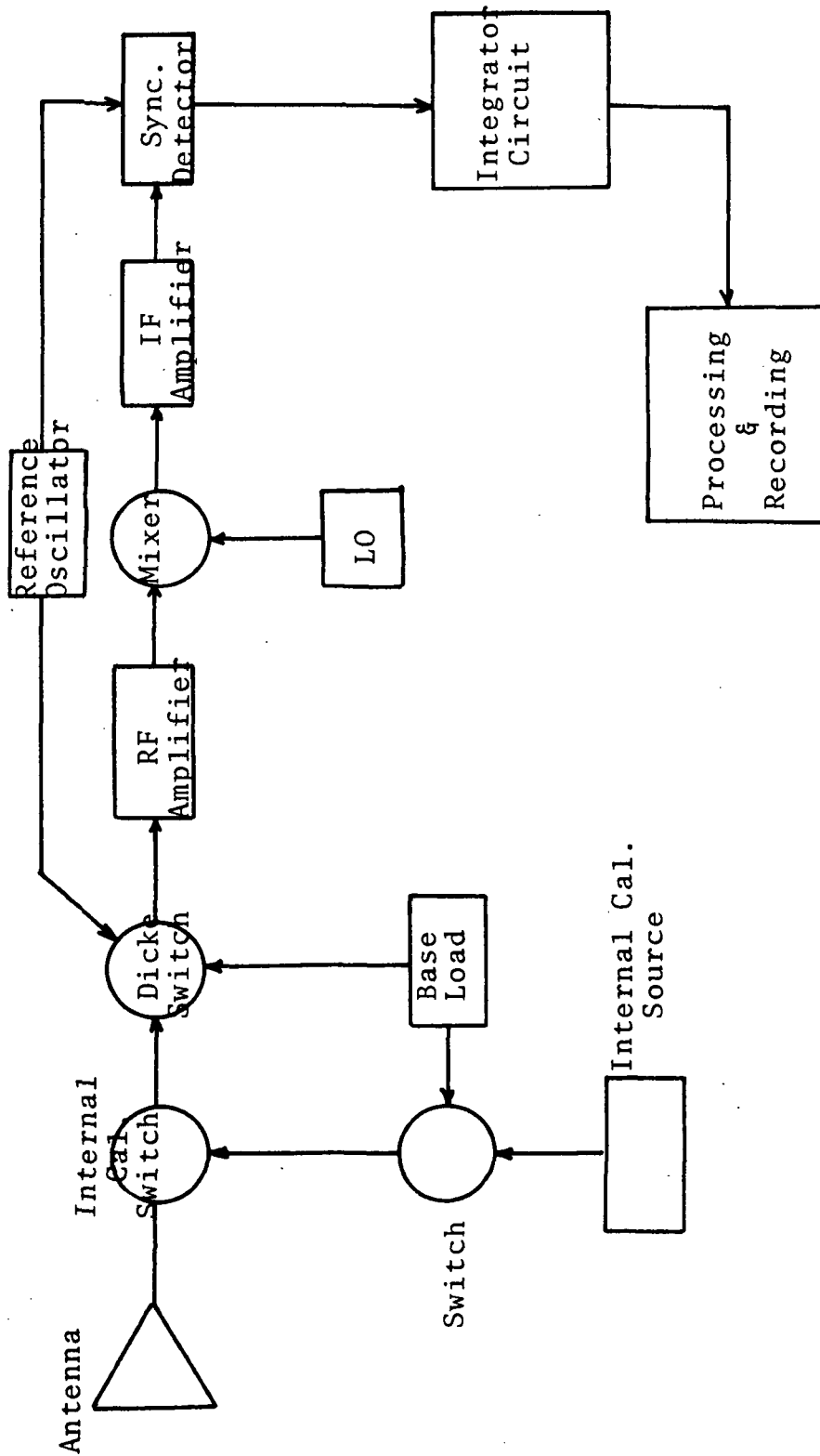


Fig. II-1. System diagram for a typical Dicke radiometer.

with the internal calibration which gives the slope or difference in temperature scale, the absolute reading for a single temperature provides a zero intercept, thus completing the calibration procedures.

The receiver sensitivity of a microwave radiometer is defined as the rms fluctuation of the output signal when a constant reference load is applied at the input. The sensitivity, ΔT , is composed of statistical fluctuations and amplifier gain variations and is given by [25]

$$\Delta T = \frac{C(F-1)}{\sqrt{B\tau}} + \frac{G(t)-G_0}{G_0} (T_\ell' - T_{ant}) \quad (\text{II-9})$$

where: C = constant depending on system parameters
 T_ℓ = reference load temperature
 T_ℓ' = load temperature referred to mixer input
 T_{ant} = effective antenna temperature
 F = system noise figure
 B = detection bandwidth
 τ = postdetection integration time
 $G(t)$ = instantaneous gain
 G_0 = average value of gain

The first term of (II-9) is caused by statistical fluctuations of the output due to the noise added to the signal by the front end of the radiometer. The second

term is caused by the gain variations of the amplifiers. Depending on the design and intended use of a radiometer, either term could dominate the other. If the radiometer were to be used in a fixed position with a stationary target, the integration could be selected as large as desired to reduce the statistical fluctuations term of (II-9) to a negligible figure. However, when the radiometer is employed in a non-stationary situation, the statistical fluctuation term is often dominant because the integration time is restricted.

When applying the radiometer in airborne operations, special system characteristics must be considered. When observing an object with finite dimensions, the viewing time of a target becomes an upper bound on the integration time. With a small integration time, τ , the sensitivity of the radiometer is assumed to be dependent solely on the statistical fluctuation term and (II-9) becomes

$$\Delta T = \frac{C(F-1) T_g}{\sqrt{B\tau}} \quad (\text{II-10})$$

or

$$\Delta T = S/\sqrt{\tau} \quad (\text{II-11})$$

where: $S = C(F-1) T_g/\sqrt{B} = \text{constant}$

In order to effectively monitor a target of length L from an aircraft, the radiometer antenna beam and the height and velocity of the aircraft must be considered, in addition to sensitivity. Jean [10] gives the distance, L , which is viewed by a radiometer mounted in an aircraft as

$$L = vt + h[\tan(\theta + \phi) - \tan(\theta - \phi)] \quad (\text{II-12})$$

where: v = velocity of the aircraft

t = viewing time

h = altitude of the aircraft

θ = viewing angle of the radiometer with respect to nadir

ϕ = one half the beamwidth of the radiometer antenna

or
$$L = vt + hA \quad (\text{II-13})$$

where: $A = \tan(\theta + \phi) - \tan(\theta - \phi)$

If at least one apparent temperature reading is desired from an area of length L , then the integration time, τ , of the radiometer cannot be greater than the viewing time, t . Solving (II-13) for the viewing time, t , gives

$$t = L/v - (h/v)A \geq \tau \quad (\text{II-14})$$

and recalling (II-11) for the sensitivity constraints of

the integration time

$$\Delta T = S/\sqrt{T} \quad (\text{II-11})$$

In (II-11) and (II-14) the basic system parameters are related in terms of the constants A and S, figures of merit for the radiometer antenna and receiver, respectively. Closer examination reveals that the choice of the receiver integration time must be based on a trade-off between temperature sensitivity, ΔT , and spatial resolution, represented as L, for a given altitude and velocity. An excellent discussion of the system trade-offs involved in airborne radiometer measurements along with a methodical procedure for evaluating operational capabilities is given by Jean [10]. An additional discussion of radiometer performance with application trade-offs is given by Schanda [26].

Perhaps the most overlooked sources of error in apparent temperature measurements are those errors stemming from non-ideal antennas. Antenna discrepancies can be divided into two categories: 1) errors resulting from non-ideal antenna patterns, and 2) system limitations due to fluctuations in antenna pointing.

Consider a radiometer antenna with an antenna power pattern given by $f_k(\Psi, \xi)$ where Ψ and ξ are polar azimuth angles, respectively, and k represents the polarization.

If the radiometer antenna is illuminated by radiation of brightness temperature $T_B^k(\psi, \xi)$, then the corresponding antenna temperature, T_a^j , is [27]

$$T_a^j(\theta_0) = \frac{\int f_V(\psi, \xi) T_B^V(\psi, \xi) d\Omega + \int f_H(\psi, \xi) T_B^H(\psi, \xi) d\Omega}{\int f_V(\psi, \xi) d\Omega + \int f_H(\psi, \xi) d\Omega} \quad (\text{II-15})$$

where: V = vertical polarization

H = horizontal polarization

j = desired received polarization, either vertical or horizontal

In well designed antennas, the design polarization state, j, is significant over the main beam, but the orthogonal polarized term may contribute a non-negligible fraction of the total received power in the side-lobes and back-lobes (e.g., 2%) [27].

The antenna temperature $T_a^i(\theta_0)$ is the power collected by the antenna and processed by the receiver. However, in most cases the quantity desired is

$T_B^j(\psi=0) = T_B^j(\theta_0)$, the brightness temperature of the radiation incident along the main beam direction of the antenna. A direct solution for $T_B^j(\theta_0)$, using (II-15) is rarely performed. Several methods are used to calculate $T_B^j(\theta_0)$ which avoid the inversion process, the simplest of which involves a side-lobe correction procedure. Estimates are made of the beam efficiency and the power

entering the antenna via the side- and back-lobes, giving reasonably accurate estimates of $T_B^j(\theta_0)$, if the beam efficiency is high.

In some operations, the limiting factor in system performance may be determined not by the inherent precision of the radiometer, but by deviations introduced by fluctuations in look angle or atmospheric path loss variations. Consider a small target contributing brightness temperature $T_t(\theta)$ to the antenna temperature with the antenna having a rms fluctuations of $(\overline{d\theta})^2$ in look angle due to vehicle oscillation or antenna steering control system. The total fluctuations in antenna output (ΔT_a) are approximated as [27]

$$\Delta T_a \approx \left\{ (\Delta T)^2 + \left[\frac{\partial T_t(\theta)}{\partial \theta} \right]^2 (\overline{d\theta})^2 \right\}^{1/2} \quad (\text{II-16})$$

where: ΔT = sensitivity of the radiometer

If the target is uniform, then $\frac{\partial T_t(\theta)}{\partial \theta}$ will be small and the overall sensitivity will closely conform to the receiver sensitivity ΔT . However, for abrupt variations of $T_t(\theta)$ the receiver sensitivity may be unattainable. If the surface has a temperature T_b and the atmosphere has physical temperature T_{atm} and attenuation α between surface and radiometer, then the antenna temperature is approximately

$$\bar{T}_a = (1 - \alpha)\bar{T}_b + \alpha T_{atm} \quad (\text{II-17})$$

and fluctuation in T_a is approximately [27]

$$(\Delta T_a)^2 \approx (\Delta \alpha)^2 (\bar{T}_b - T_{atm})^2 \quad (\text{II-18})$$

Since $(\bar{T}_b - T_{atm})$ may be up to 100°K for observation of highly reflective surfaces such as water, fluctuations in α of the order of 0.04dB may introduce fluctuations on the order of 1°K in T_a [27].

This chapter has provided the framework of operation for the microwave radiometer. Working within the concepts of thermal emission and the basic detection of the emission by the sensor, Chapter III provides the tools for interpretation of the radiometer measurements for a desired observation.

CHAPTER III

INTERPRETATION OF RADIOMETRIC DATA

The Concept of Apparent Temperature

In Chapter II the basic concepts of natural radiation of an object and the subsequent detection systems for microwave frequencies were discussed. In this chapter the information content of the radiometer output is analyzed. Because the output of a radiometer is expressed as an absolute temperature, an understanding of the term known as apparent temperature is required. Paramount in the discussion of apparent temperatures is the fact that this absolute temperature measurement is in reality a measurement of power.

The apparent temperature recorded by the radiometer consists of contributions from more than just the object under observation. The power received by the radiometer antenna consists of the natural emissions of the target and any radiation which is incident upon the target surface and scattered toward the main beam of the antenna. In addition, the intervening atmosphere attenuates the net radiation from the surface, as well as introduces some natural radiation of its own directed toward the main beam. The other sources of power originate from the side

lobes of the antenna and any cross polarization components due to polarization inefficiencies of the antenna. As discussed in Chapter II, the cross polarization and side lobe contributions are normally thought to be sensor system parameters, and many of the errors due to the sensor itself are corrected in the calibration procedures.

In Chapter II it was shown that the target radiation is equal to the emissivity, ϵ , times the physical temperature of the target, T_g . The emissivity is in general a function of frequency, polarization, angle of observation (or look angle), surface roughness, and the complex permittivity of the target.

The radiation from the upper hemisphere incident on the target surface is normally referred to as sky radiation. The reflected portion of the sky radiation directed toward the radiometer antenna, T_r , can be found using the bistatic scattering coefficients, $\sigma_{ij}(\theta_o, \phi_o; \theta_s, \phi_s)$, as

$$T_r^j(\theta_o, \phi_o) = \iint \left[\sigma_{jj}(\theta_o, \phi_o; \theta_s, \phi_s) + \sigma_{jk}(\theta_o, \phi_o; \theta_s, \phi_s) \right] \frac{T_s(\theta_s, \phi_s)}{4\pi \cos \theta_o} d\Omega_s \quad (\text{III-1})$$

where: $T_s(\theta_s, \phi_s)$ = sky radiation incident on the target from direction θ_s, ϕ_s

j, k = the orthogonal polarizations states, vertical and horizontal

θ_o, ϕ_o = look angle and azimuth, respectively

and the integration is over the upper hemisphere. The inherent assumption in (III-1) is the unpolarized nature of the sky radiation, $T_s(\theta_s, \phi_s)$.

The net radiation from the surface, which is composed of the target radiation and the reflected sky radiation, is reduced by a factor of $a(r)$, which is the atmospheric attenuation factor for the received signal a distance r meters from the target, given as

$$a(r) = \exp\left[-\int_0^r \alpha(\rho) d\rho\right] \quad (\text{III-2})$$

where: $\alpha(\rho)$ = attenuation of the atmosphere in nepers/meter along the line of sight from the target to the receiver

The atmosphere between the target and the radiometer also contributes an amount of radiation directed toward the antenna main beam. This radiation is known as T_{path} , which is given by [27]

$$T_{\text{path}} = \int_0^r T_m(\rho) e(\rho) \left[\frac{a(r)}{a(\rho)} \right] d\rho \quad (\text{III-3})$$

where: $T_m(\rho)$ = physical temperature of the atmosphere

$e(\rho)$ = emission coefficient per meter of the atmosphere

If losses due to scattering of the atmosphere are small compared to losses of absorption, then $e(\rho) = \alpha(\rho)$, which is a reasonable assumption at microwave frequencies and

for clear weather conditions. The atmospheric attenuation and absorption coefficients $e(\rho)$ and $\alpha(\rho)$ are assumed to be independent of polarization.

Since natural radiation is incoherent, the various contributions add directly to give the total apparent temperature, T_a^j , as [27], [28], [29]

$$T_a^j(\theta_0, \phi_0) = a(r) \left\{ \epsilon_j(\theta_0, \phi_0) T_g + \iint \left[\sigma_{ij}(\theta_0, \phi_0; \theta_s, \phi_s) + \sigma_{jk}(\theta_0, \phi_0; \theta_s, \phi_s) \right] \frac{T_s}{4\pi \cos \theta_s} d\Omega_s \right\} \quad (\text{III-4})$$

$$+ \int_0^r T_m(\rho) e(\rho) \left[a(r)/a(\rho) \right] d\rho$$

Models

The approach to evaluating (III-4) was first presented by Peake [28], and later Peake and Chen [29], Strogyn [30], and Ulaby et al. [31]. This method evokes a generalized form of Kirchhoff's radiation law using the assumption of thermal equilibrium between the surface and a blackbody half-space above. The emissivity, $\epsilon_j(\theta_0, \phi_0)$, is shown to be equal to the absorptivity, $a_j(\theta_0, \phi_0)$, hence the emissivity is equal to one minus the albedo, the ratio of power scattered from a surface in a particular direction to the total incident power on the surface, or

$$\epsilon_j(\theta_0, \phi_0) = 1 - \iint \left[\sigma_{jj}(\theta_0, \phi_0; \theta_s, \phi_s) + \sigma_{jk}(\theta_0, \phi_0; \theta_s, \phi_s) \right] \frac{d\Omega_s}{4\pi \cos \theta_0} \quad (\text{III-5})$$

The emissivity is now dependent solely on the scattering coefficients of the surface, which can be obtained empirically using radar. This approach is commonly referred to as Peake's model for apparent temperatures.

An alternate approach to the modeling of thermal emissions is given by Johnson [32]. Rather than equating emission to absorption for the surface by means of assuming thermal equilibrium of the surface radiator and its surroundings, Johnson's model requires only that thermal equilibrium exist within the homogeneous and isotropic substance under observation. The internal radiation of the medium is described by its intrinsic spectral emissivity and its physical temperature. The internal radiation is incident on the surface, and the portion of the radiation which is transmitted toward the radiometer is found using the transmissive scattering coefficients for the boundary and the effective scattering area in the direction of the antenna. It is interesting to note that Johnson's model reduces to Peake's model for the special case of a radiating medium in thermal equilibrium with its surroundings [32].

Surface Roughness and Vegetation Effects

In any of the models for radiometric interpretation there must be included a means of determining the effect of the scattering boundary which constitutes the surface. Radiation from a medium is emitted according to the shape and dielectric properties of the boundary. In addition, the contribution of the apparent sky temperature is a result of the scattering properties of the surface and the incident radiation from the sky.

The parameters which are used to describe the surface (and sometimes subsurface) effects are the scattering coefficients (or in the case of Johnson's model, the transmissive scattering coefficients). The scattering coefficients simply relate the energy incident from a particular direction (θ_s, ϕ_s) on the surface to the energy scattered in the direction of interest, i.e. the look angle of the sensor (θ_o, ϕ_o) . The scattering coefficients, dependent on the complex permittivities of the two media forming the boundary, are conceded to be known for only the purely specular or diffuse cases. The smooth surface assumption gives rise to a purely specular component of the scattered field, while the Lambert approximation of purely diffuse scattering indicates a surface which scatters radiation equally well in all directions. Unfortunately, very few natural surfaces at microwave

frequencies exhibit either smooth surface or Lambertian surface scattering properties. Most terrestrial surfaces have variations such that at microwave frequencies they must be viewed as random rough surfaces.

The development of theories of scattering from randomly rough surfaces has been addressed, by nature of its complexity, from various approaches, each of which having certain simplifying assumptions. One such group is the class of surfaces whose variations are large compared with the wavelength of interest, and the complement is the class of surfaces where the roughness is considered small when compared to a wavelength. A composite surface approach combines the results of both large and small scale roughness to give an even better approximation of the scattering phenomenon at a cost of higher complexity. Another approach to rough surface scattering has been to approximate the surface using known geometrical shapes. A rather extensive compilation of rough surface scattering can be found in Ruck, et al. [33].

In observing terrestrial surfaces one is often faced with more than just a single rough boundary. Recent attention has been focused on the modeling of vegetated terrain as a surface scatterer. Peake [34] has modeled stemmed crops such as wheat by viewing the crop as randomly slanted long dielectric cylinders. Peake and

Oliver [27] have used a volume scattering approach for dense vegetation cover by assuming a random arrangement of dielectric discs, known as the Lommel-Seeliger model, and Sibley [35] has addressed the problem of dielectric layering of crop upon soil for geometrical shapes which would be normally found in agricultural fields, such as standard row crops.

Although agreement on a satisfactory description of scattering from natural surfaces is lacking, the rough surface descriptions agree on two basic characteristics: 1) the scattered fields are a function of the electromagnetic characteristics (complex permittivities) of the media forming the boundary, and 2) the scattered fields are a function of average roughness parameters [15].

The scattering properties of a surface are related to the emissivity of the surface by both Peake's model and Johnson's model for radiometric measurements, therefore the scattering properties are important in passive microwave monitoring of soil moisture.

Application to Soil Moisture Detection

Within any means of determining scattering coefficients or transmission coefficients, the complex

permittivities* of the two media forming the boundary must be included. Since the relative dielectric constant, ϵ_r , of dry soil for microwave frequencies is normally from 3 to 5, and for the same frequencies the dielectric constant for water can be as high as 80, a mixture of soil and water would appear to have a dielectric constant somewhere in between the two extremes, depending on the relative proportions of the mixture. The differences in dielectric constant affect the scattering and transmission coefficients which in turn are used in determining the emissivity of the mixture and the albedo of the surface. Figure III-1 shows the complex dielectric constant of sand for varying moisture constants measured at frequencies of 1.49, 9.0, and 31.4 GHz.

For purposes of illustration, the smooth surface approach is used to express the emissivity as a function of look angle in Figure III-2 for three separate moisture values. The smooth surface emissivities are found using the Fresnel reflection coefficients, R_j , as [27]

$$\epsilon_j(\theta_o) = 1 - |R_j(\theta_o)|^2 \quad (\text{III-6})$$

where R_j represents the Fresnel reflection coefficient

*Assuming a constant permeability equal to free space permeability.

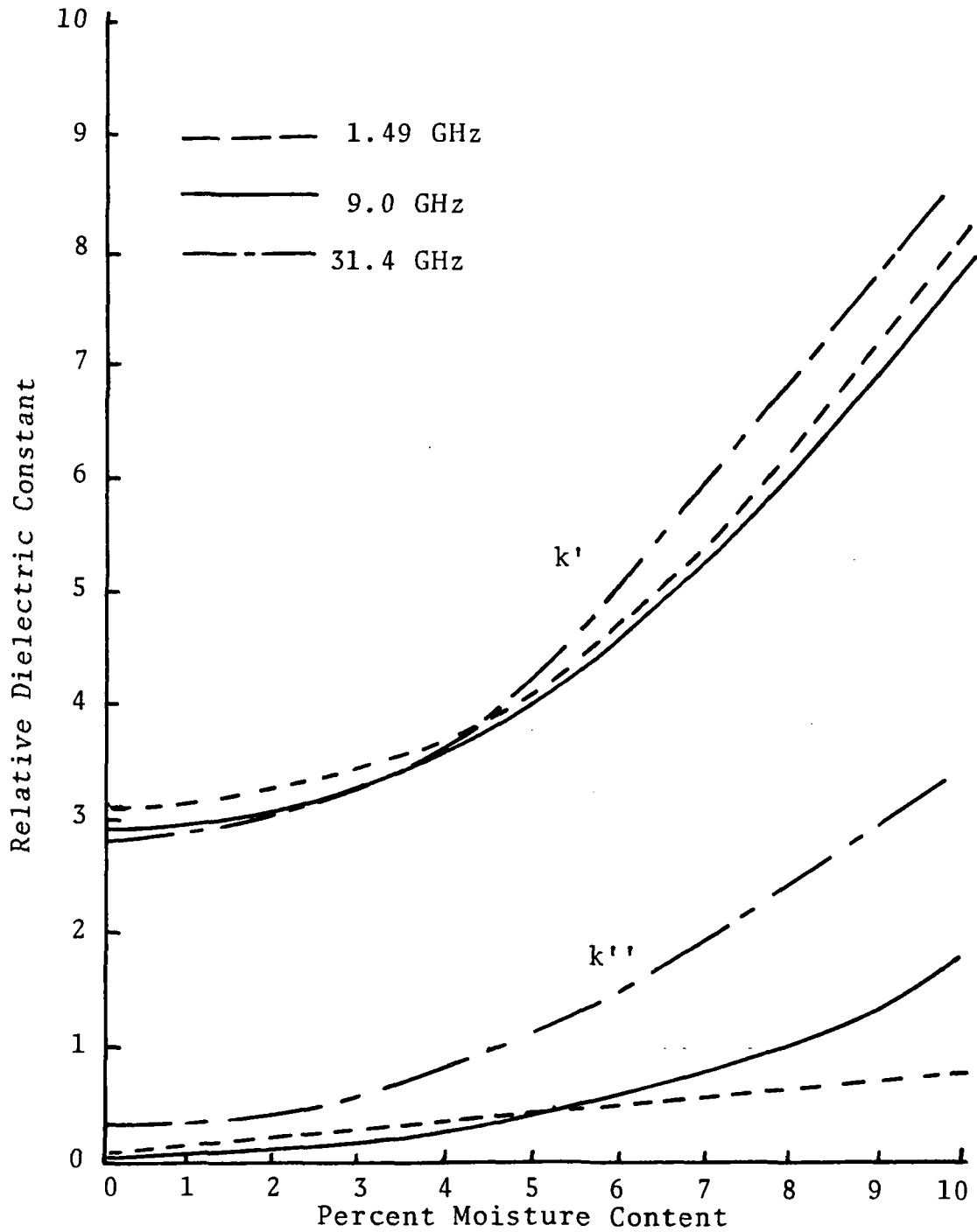


Fig. III-1. Relative complex dielectric constant for sand versus moisture content [41]

with polarization j and [27]

$$R_V(\theta_0) = \frac{k_c \cos \theta_0 - \sqrt{k_c - \sin^2 \theta_0}}{k_c \cos \theta_0 + \sqrt{k_c - \sin^2 \theta_0}} \quad (\text{III-7})$$

$$R_H(\theta_0) = \frac{\cos \theta_0 - \sqrt{k_c - \sin^2 \theta_0}}{\cos \theta_0 + \sqrt{k_c - \sin^2 \theta_0}} \quad (\text{III-8})$$

where: V and H represent the vertical and horizontal polarizations, respectively

k_c = relative complex dielectric constant

Figure III-2 shows the emissivity of a smooth surface as a function of incidence angle. For horizontal polarization, the emissivities decrease for larger angles of incidence. The emissivities for the vertically polarized cases increase with increasing incidence angle to a maximum occurring at the Brewster angle. The incidence angle at which the Brewster angle occurs shifts toward grazing for higher percent moisture content. Figure III-3 shows the emissivity as a function of percent moisture content for look angles of 0° , 38° , and 75° from nadir. Due to the Brewster angle effect, the emissivities at the 75° look angle increase with increasing moisture content, but generally the emissivities decrease when the percent moisture content increases for look angles of less than 60 degrees.

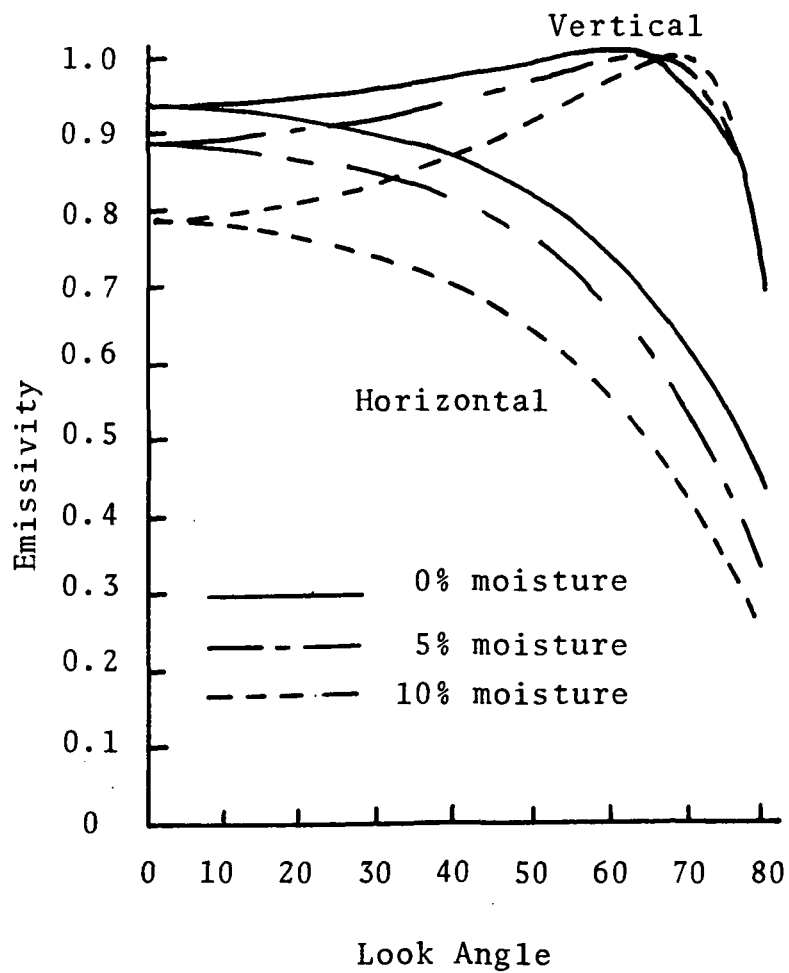


Fig. III-2. Emissivity as a function of look angle.

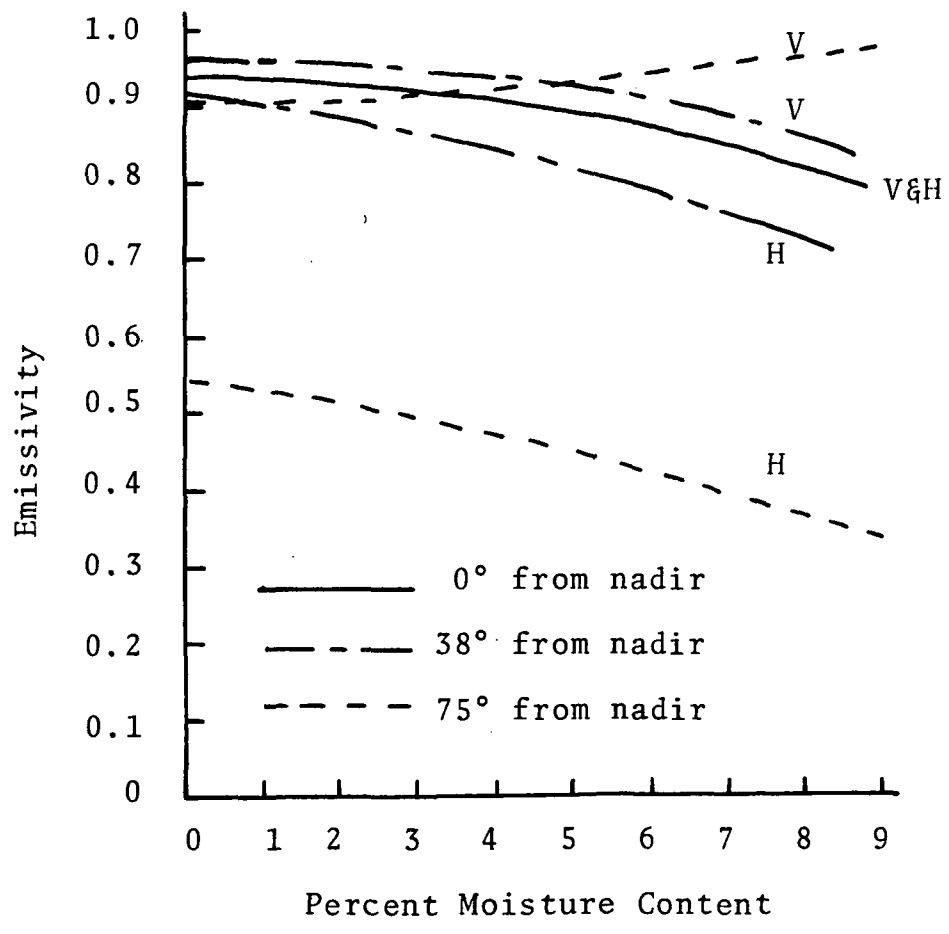


Fig. III-3. Emissivity as a function of moisture content.

Consider a radiometer monitoring a field at a wavelength long enough as to render the smooth surface approximation valid. For microwave frequencies below 4 GHz Paris [5] indicates the atmospheric attenuation and radiation have negligible contribution to the apparent temperature and (III-1) becomes

$$T_a^j(\theta_0) = \epsilon_j(\theta_0, \phi_0) T_g + \iint \left[\sigma_{ij}(\theta_0, \phi_0; \theta_s, \phi_s) + \sigma_{jk}(\theta_0, \phi_0; \theta_s, \phi_s) \right] \frac{T_s}{4\pi \cos \theta_s} d\Omega_s \quad (\text{III-9})$$

Since galactic sources of microwave energy reaching the earth's surface are low and the atmospheric radiation has already been indicated as negligible for the longer wavelength, (III-6) can be further simplified by assuming the reflected sky radiation has negligible contribution to the apparent temperature, leaving

$$T_a^j(\theta_0) = \epsilon_j(\theta_0) T_g \quad (\text{III-10})$$

or rearranging (III-10)

$$\epsilon_j(\theta_0) = T_a^j(\theta_0) / T_g \quad (\text{III-11})$$

Clearly the assumptions used to obtain (III-11) are not completely valid, however, if the system and surface parameters are such that these assumptions can be employed, a basis for radiometer data interpretation exists in (III-11). Therefore, if the complex dielectric

constant-soil moisture content curve is available for the soil(s) under observation, a reliance on (III-11) can predict the apparent temperatures of fields with varying moisture contents to a first approximation. Later the assumptions can be relaxed for finer interpretation.

Current and future development of passive microwave capability to measure soil moisture depends heavily on experimental data. Much of the available data has been obtained using radiometers operated by the National Aeronautics and Space Administration. Two NASA aircraft, the CV-990 and the NP-3A, have provided airborne radiometer data. The NP-3A is equipped with an X-band scanning radiometer known as PMIS (Passive Microwave Imaging Sensor) and a set of four constant look angle radiometers operating in the L, X, K, and Ka bands. The CV-990 aircraft was destroyed in a tragic airplane collision in April, 1973.

A ground based system of dual frequency radiometers is scheduled for operation by NASA Johnson Space Center in the summer of 1973. These L-band and X-band radiometers are to be mounted to the boom of a truck for field studies.

CHAPTER IV

SOILS AS DIELECTRICS

From Chapter III it was determined that to predict the moisture content of soils using passive microwave sensors, a knowledge of the soil complex permittivities for varying percent moisture contents is needed. Before trying to evaluate the dielectric properties of soil some feeling of the material under examination must be known. As is often the case between two separate disciplines, little interaction of the fields of soil sciences and electrical engineering exists. Most studies of dielectric properties of soil have been made at low frequencies, and the work to date with regard to soil permittivities at microwave frequencies has been done by engineers and not the soil scientists. This chapter is divided into two sections. An introduction to soil systems is given in the first section to provide a working knowledge of the terminology and concepts used by the soil scientist. The second section develops the approach to measuring the soil complex permittivity.

Introduction to Soil Systems*

The soil is a highly complex, living system, existing in three phases. The solid phase includes the soil particles, the liquid phase encompasses the soil water and dissolved substances, and the gaseous phase consists of soil air. The solid matrix consists of soil particles differing in chemical composition as well as in size, shape, and orientation. The mutual arrangement of the particles of the soil determines the pore spaces and passages in which the soil fluids are retained and transmitted. The soil structure is highly dynamic and may vary greatly in response to changes in natural conditions, biological activity, and soil-management practices.

Soil particles are divided into types according to size. As shown in Figure IV-1, the largest soil particles, sand, are from 0.05 mm to 2.0 mm in diameter, particles of silt are from 0.002 mm to 0.05 mm in diameter, and clay particles have a diameter smaller than 0.002. Silt and sand particles generally approximate spherical or cubical shape, whereas the smaller clay particles are plate or lath shaped, according to the crystal structure of the

*Much of the discussion in this section can be found in greater detail from two volumes by Kohnke [36] and Hillel [37].

Diameter (mm)	
2.0	Very coarse sand
1	Coarse sand
0.5	Medium sand
0.25	Fine sand
0.1	Very fine sand
0.05	
	Silt
0.002	
	Clay

Fig. IV-1. USDA fractionation of soil particles [36].

type of clay. The very smallest soil particles have no uniform shape, and hence are amorphous.

Within any representative quantity of soil there can exist all three soil types in various relative proportions. The textural classification is determined by the percentage of each of the three soil types. Figure IV-2 shows the soil-texture triangle, which designates the textural classification of a soil based on a percentage scale of the relative amounts of each of the three soil separates. Textural designations are designated by using the names of the predominant size fractions and the word loam whenever all three major size fractions occur in sizeable proportions. The USDA soil-texture triangle is calculated on the basis of organic-free, oven-dry soil particles less than 2 mm in diameter. Soil containing over 15 percent organic matter are designated as mucky or muck for well decomposed material, and peaty or peat for soils with only partially decomposed plant residues.

The specific surface of soil is important because the chemical and physical activities which take place occur mainly at the surface of the particle, therefore the specific surface is approximately proportional to the amount of these activities. Figure IV-3 shows the relationship between the particle size of soil fractions and their approximate specific surfaces. Since the particle

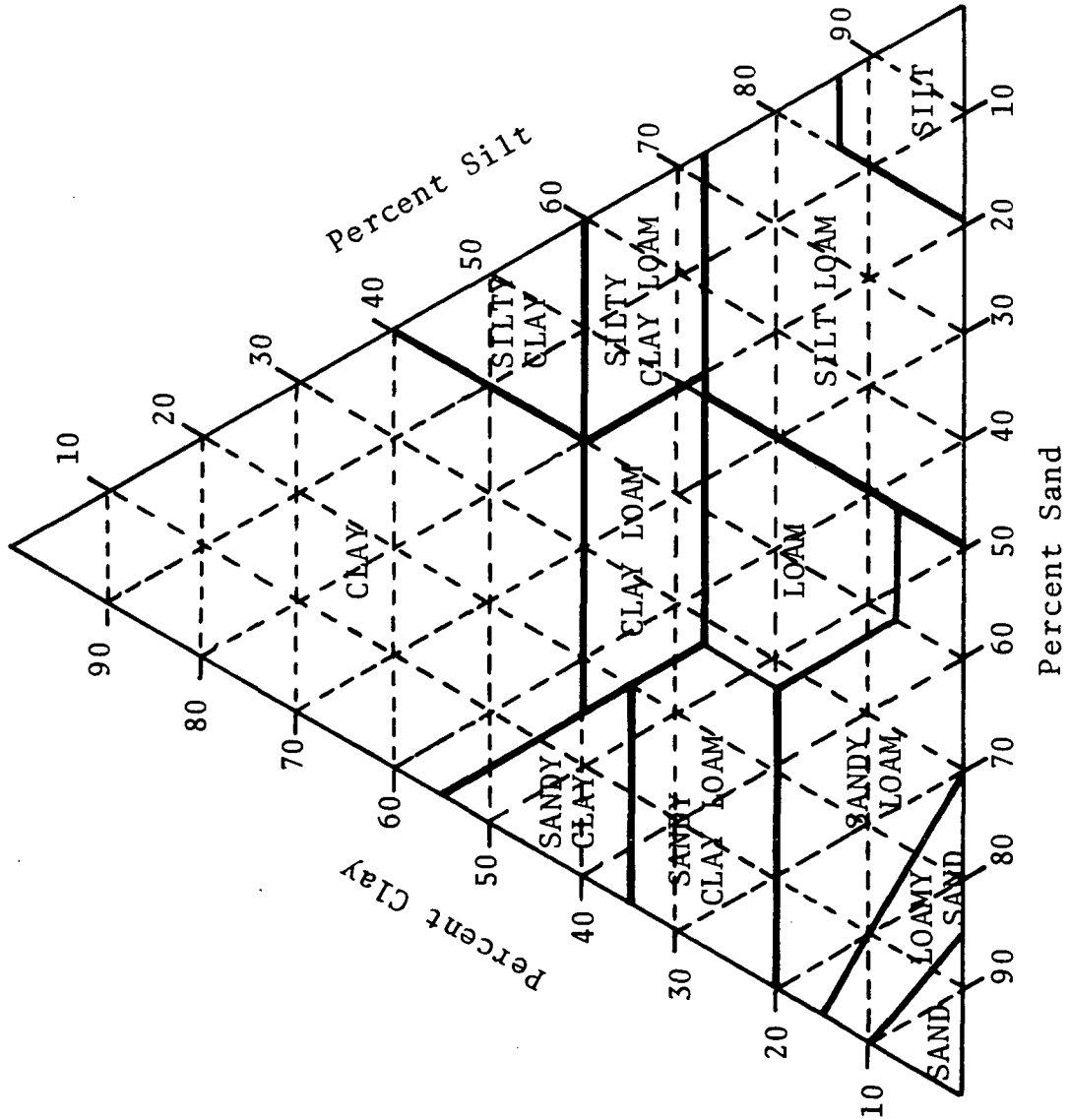


Fig. IV-2. Soil textural triangle

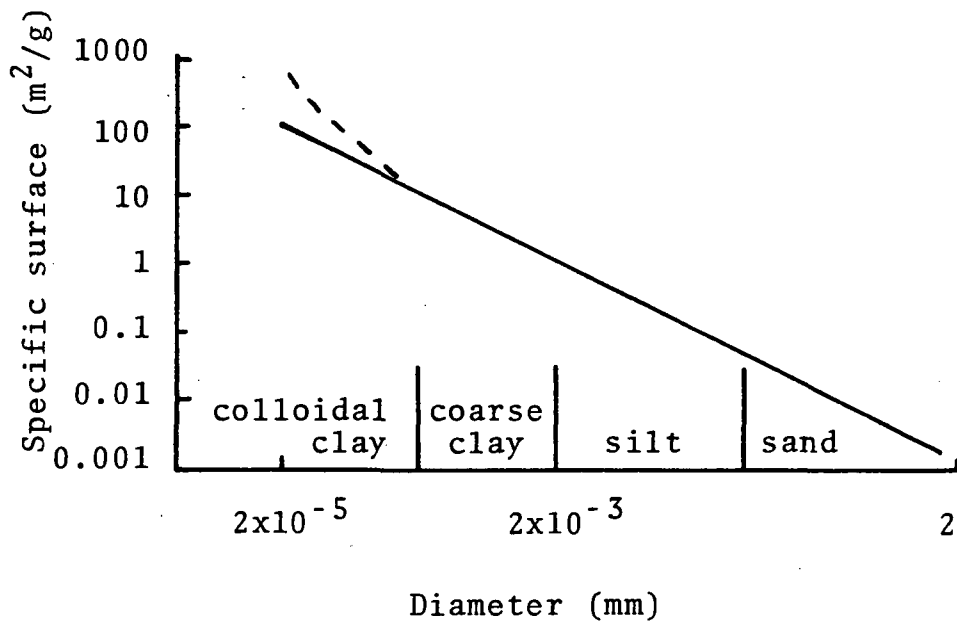


Fig. IV-3. Specific surface versus particle diameter [36].

diameter (mm) and specific surface (m^2/gram) are shown to be inversely related on a logarithmic scale, the smaller clay fractions, while only occupying perhaps 20 percent of the soil by weight, account for practically the total specific surface. Moisture holding capacity of soils is dependent on the total surface area of the soil, thus a soil with a significant clay content can retain a high level of moisture before reaching saturation.

Before describing the ways in which water is retained by the soil, a discussion of the water molecule itself and its attraction to other water molecules should be included. The water molecule consists of two hydrogen atoms bonded to a single oxygen atom, forming an angle of approximately 105° . The electron cloud is displaced more toward the more positively charged oxygen nucleus, thus causing a dipole moment to exist within the molecule. This dipole moment causes electrostatic attraction of the more positive hydrogen atoms to the more negative oxygen atom of another molecule. This attraction, called hydrogen bonding, causes water to exist as a string of molecules, or a polymer. The electrostatic attraction between the soil particles and water molecules also produces hydrogen bonding. When the affinity for hydrogen bonding between the water and the soil particles is great, the polymer structure of water is reduced, and when the soil

particles are saturated, the excess water molecules resume their polymer structure.

The soil scientist defines the affinity for hydrogen bonding of the soil particles and water molecules as soil moisture tension. The soil moisture tension is equal to the pressure difference between moisture held in the soil and free water. Tension is expressed in pF as [36]

$$pF = \log_{10} h \quad (IV-1)$$

where h is the pressure difference expressed in centimeters of water.

Soil moisture is classified according to the tension at which it is held by the soil. Table IV-1 summarizes the types of soil moisture and the tension at which they are retained by the soil.

There are two methods of expressing soil moisture. The soil moisture tension is one method, and the actual amount of water by weight as a percentage of the total dry weight of the soil is the second method. The present-day dry weight determination of soil moisture is measured by weighing a sample of soil, then heating the sample (commonly at 105°C) until it has reached the vapor equilibrium of the oven, and reweighing. The percent soil moisture content is expressed as

TABLE IV-I

CLASSIFICATION OF SOIL MOISTURE pF

Water of constitution and interlayer water	Above 7.0
Hygroscopic water	7 - 4.5
Capillary water	4.5 - 2.5
Gravitational water	2.5 - 0
Ground water	Tension free

$$\% \text{ Soil Moisture} = \frac{W_t - W_{od}}{W_{od}} \times 100 \quad (\text{IV-2})$$

where: W_t is the total weight of the moist sample and
 W_{od} is the weight of the oven dry soil

Drying of the soil in an oven set at 105°C will release all soil moisture except the water of constitution.

Cohesion and adhesion are the two forces that hold the soil-water system together. Cohesion is a result of the mutual attraction of soil particles brought about by surface charges of clay particles. For very low values of soil moisture, cohesion is strong due to the large amount of interfacial contact of the particles, however as the moisture of the soil increases the interfacial areas become separated by water and cohesion decreases. Adhesion depends on the presence of both water and air in proper amounts. It is a film force between the soil particles and the water. Adhesion reaches a maximum for soils in the fairly wet range but decreases to almost nothing in very wet and saturated soils.

Measurement of the Complex Dielectric Constant

The complex permittivity, the electromagnetic property of the soil which provides a link between soil moisture and radiative properties, is defined by using the

basic principles of Maxwell, i.e.

$$\nabla \times \bar{H} = \frac{\partial \bar{D}}{\partial t} + \bar{J} \quad (\text{IV-3})$$

Normally, the profile of a soil will reveal rather large differences in texture and structure, however, for observing emission in the microwave wavelengths (≤ 30 cm), only the material within several wavelengths is considered to have significant contribution. For purposes of this study, the soil is considered to be homogeneous topsoil. In addition, the soils measured were disturbed from their original state and therefore must be considered as isotropic, homogeneous medium. With $e^{j\omega t}$ variation and applying Ohm's law (IV-3) becomes

$$\nabla \times \bar{H} = j\omega \epsilon \bar{E} + \sigma \bar{E} \quad (\text{IV-4})$$

where $\epsilon \bar{E}$ (the permittivity times the electrical field vector) replaces \bar{D} (the electric flux density) and σ is the scalar conductivity. Combining like terms in (IV-4) gives

$$\nabla \times \bar{H} = [j\omega \epsilon + \sigma] \bar{E} \quad (\text{IV-5})$$

Factoring $j\omega$ from the brackets leaves

$$\nabla \times \bar{H} = j\omega \left[\epsilon + \frac{\sigma}{j\omega} \right] \bar{E} \quad (\text{IV-6})$$

The expression in the brackets is combined into a single term called the complex permittivity, ϵ_c , and is commonly written

$$\epsilon_c = \epsilon' - j\epsilon'' \quad (\text{IV-6})$$

where: ϵ' is the real part of the complex permittivity
 ϵ'' is the imaginary part of the complex permittivity

For convenience, ϵ_0 , the free space permittivity, is factored from (IV-6) giving

$$k_c = k' - jk'' \quad (\text{IV-7})$$

where: $k_c = \epsilon_c / \epsilon_0 =$ relative complex dielectric constant

With the ubiquitous nature of water, any study of terrestrial permittivities requires that some estimates of the complex permittivity for water be available. The complex permittivity for fresh water and ice is given as [25]

$$\epsilon_c = \epsilon^\infty + \frac{\epsilon_d - \epsilon^\infty}{(1 + jf/f_0)} - j \frac{\sigma^i}{\omega \epsilon_0} \quad (\text{IV-8})$$

where: $\epsilon^\infty = 5.5$

$\epsilon_d = 87.7 - 0.4$ (temperature in $^\circ\text{C}$)

$f_0 = 9.1$ GHz for water at 273°K

$f_0 = 12.6$ GHz for water at 283°K

$$f_o = 17.2 \text{ GHz for water at } 293^\circ\text{K}$$

$$\sigma^i = \text{ionic conductivity}$$

$$f = \text{frequency in hertz}$$

Values for the complex dielectric constant of sea water vary widely. For a comprehensive treatment of the complex dielectric constants for water see Paris [5].

The dielectric properties of soils have been studied by various investigators at microwave wavelengths. Hertel, et al. [38] reports determination of dielectric constants at 8.6 mm wavelength by propagating a wave through a sample of known thickness in free space, and measuring the attenuation and phase shift deviations of the signal from a reference source of the same origin. Lundien [39] has made extensive measurements of soils with an L-band interferometer, and Richerson [15] measured the complex permittivity of sand at 31.4 GHz. Wiebe [40] investigated a method of measuring the complex permittivity at X-band by inserting a soil sample inside a section of waveguide. The measurement techniques were fundamentally those of Hertel, et al. [38], with the correct modifications for propagation of guided waves. Concluding that the waveguide technique gave accurate measurements, Wiebe [41] then reported a series of X-band measurements for selected Texas soils with varying moisture contents. Vickers and Rose [42] investigated the use

of free space reflection measurements at X-band to compute the complex permittivity of terrestrial materials, and Poe, et al. [17] have reported the complex permittivities of a soil with varying moisture content as found using an ellipsometer.

The waveguide method used by Wiebe [40], [41] was selected for use in measuring the complex permittivities of the soils in this study. Since the primary frequencies of interest in observing soil moisture content using microwave radiometers are the longer wavelengths, this method provided accurate results without having the limitations of handling large soil samples present in any of the free space measurements for longer wavelengths.

In order to obtain an analytical expression for the complex permittivity, the real and imaginary parts must be expressed in measurable quantities. The propagation constant, γ , for a guided wave is given by [43]

$$\gamma = \alpha + j\beta = \sqrt{K_c^2 - K^2} \quad (\text{IV-9})$$

where: K is the wave number

K_c is the wave number evaluated at the cutoff frequency of the guide

or

$$K = \omega \sqrt{\mu(\epsilon' - j\epsilon'')} \quad (\text{IV-10})$$

and

$$K_c = \frac{2\pi}{\lambda_c} \quad (\text{IV-11})$$

where: λ_c is the cutoff wavelength

Substituting in (IV-9) gives

$$\alpha + j\beta = \sqrt{K_c^2 - \omega^2[\mu(\epsilon' - j\epsilon'')] } \quad (\text{IV-12})$$

and solving for ϵ' and ϵ''

$$\epsilon' = \frac{\beta^2 - \alpha^2 + K_c^2}{\omega^2\mu} \quad (\text{IV-13})$$

$$\epsilon'' = \frac{2\alpha\beta}{\omega^2\mu} \quad (\text{IV-14})$$

As shown previously, the real and imaginary parts of the complex permittivity, given in (IV-13) and (IV-14), respectively, are for convenience expressed as the relative complex dielectric constant, $k' - jk''$, yielding

$$k' = \frac{\beta^2 - \alpha^2 + K_c^2}{\beta_g^2} \quad (\text{IV-15})$$

$$k'' = \frac{2\alpha\beta}{\beta_g^2} \quad (\text{IV-16})$$

where: β_g is the phase constant in the waveguide

The relative complex dielectric constant is now expressed in terms of the cutoff and propagation constants of the waveguide and the attenuation and phase constants of the soil, which can be measured.

The experimental measurement design was patterned after the one described by Wiebe [40] with slight modifications. The design used, shown in Figure IV-4, is analogous to an impedance bridge at lower frequencies. An oscillator produces a 9.0 GHz signal which passes through the isolator to the 3 db directional coupler. The directional coupler divides the signal between the lower branch, with known attenuation and phase shift, and the upper branch which contains the sample. The two signals are combined with the second directional coupler and detected with a crystal detector. When the signals are of equal strength and 180° out of phase, the combination of the two causes maximum destructive interference, hence an absolute null reading from the detector.

To determine the phase and attenuation constants of a material, a known length of sample with known compaction is placed inside the waveguide sample holder, and the holder is firmly placed in the upper branch of the bridge. An absolute null is achieved for the detector output by adjusting the variable phase shifter and attenuator simultaneously. The procedure is repeated for successive

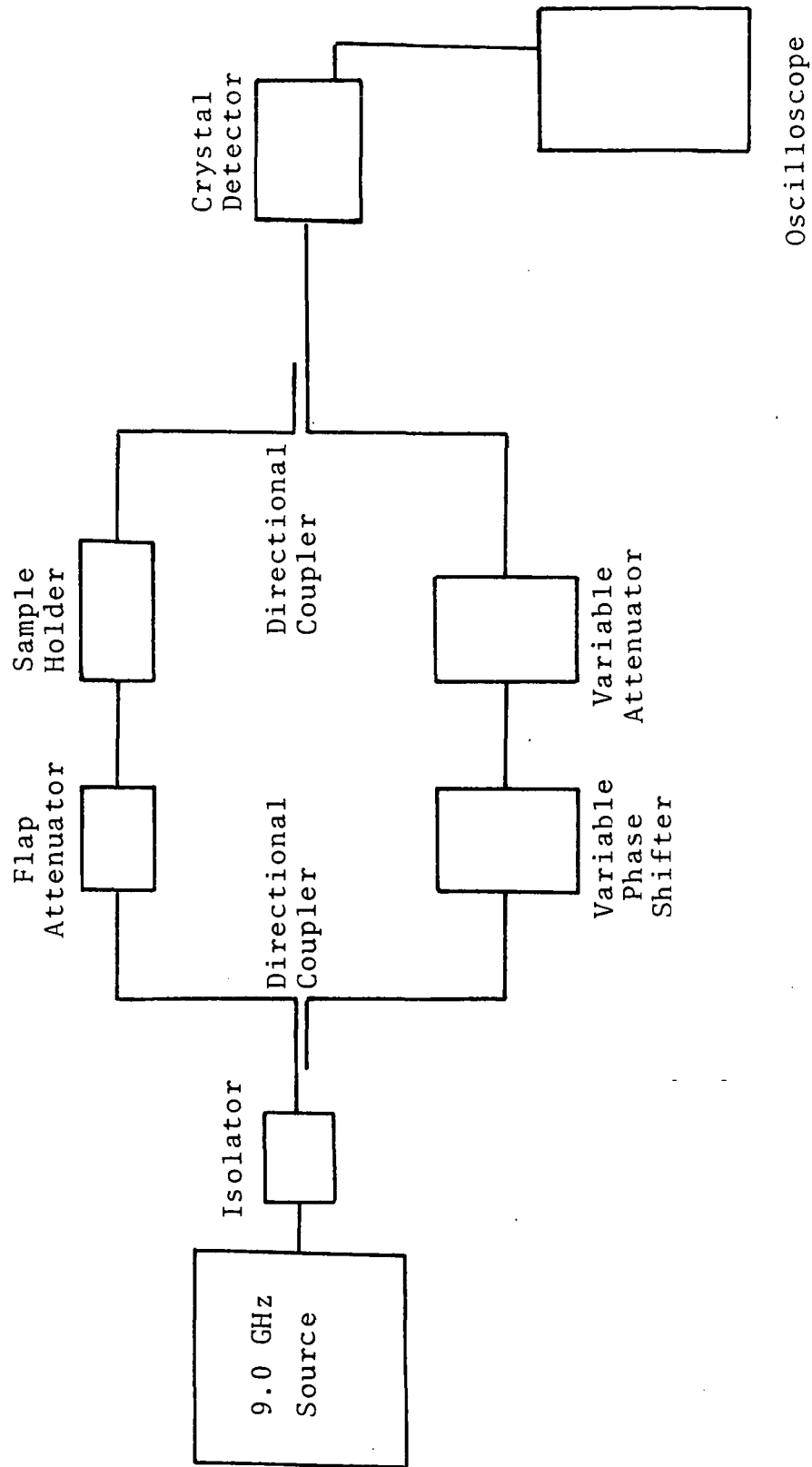


Fig. IV-4. Waveguide measurement system for determining complex dielectric constant.

changes in sample lengths, and the attenuation and phase shift measurements versus length are plotted, whose slopes are the attenuation per unit length, $\Delta\alpha_{dB}/\Delta L$, and the phase shift per unit length, $\Delta\theta/\Delta L$, respectively. The attenuation constant, α , is obtained by converting $\Delta\alpha_{dB}/\Delta L$, with dimensions of decibels per meter, to nepers per meter. The phase constant of the sample material, β , is the sum of the measured value, $\Delta\theta/\Delta L$, plus the phase constant in the waveguide, β_g , or

$$\beta = \frac{\Delta\theta}{\Delta L} + \beta_g \quad (\text{IV-17})$$

where: $\beta_g = 2\pi/\lambda_g$

and λ_g is the wavelength in the guide. With measured values of α and β , the soil's relative complex dielectric constant can be found using (IV-15) and (IV-16).

The accuracy in measuring the complex dielectric constant is limited by the length measurements of the samples. The sample lengths were measured with an accuracy of $\pm 1\text{mm}$, which corresponds to the following accuracy for the measurement of k' and k'' :

$$k' \pm 9.6\%$$

$$k'' \pm 16.5\%$$

The moisture content of the soil samples was determined using the oven dry weight basis of (IV-2). The accuracy

of the percent moisture determined in this manner has been shown to be $\pm 5\%$ [39].

The measurement procedure described above was used to determine the relative complex dielectric constants for varying moisture contents of soils from selected test sites located near Chickasha, Oklahoma and Weslaco, Texas. Wiebe [41] showed that both the compaction and the method of moistening the soil samples affected the dielectric measurements. His results using compactions of 5 and 20 Newtons/cm² showed slight increases in k' and k'' resulting for the samples prepared at 20 Newton/cm². The amount of time which the soils were allowed to sit after moistening and before measuring, denoted as the curing time of the sample, was also determined by Wiebe to affect the results of k' and k'' . Values for k' and k'' were lower for cured samples than for uncured samples because of the finite time (normally 12-24 hours, depending on the specific surface of the soil) the soil must have to absorb the water into the interfacial area of the soil particles. Once absorbed, the water molecule's freedom of movement as a dipole is restricted. Since the dielectric properties at microwave frequencies are a dipole phenomenon [43], the subsequent dielectric measurements for cured samples are reduced.

The samples used in this study were first cured for

24 hours and then compacted with a force of 5 Newtons/cm² into the sample holder. The results of all measurements are shown in Figure IV-5 with both k' and k'' plotted as a function of percent moisture content. Figure IV-6 shows the results of all silt loams and loamy soil measured, and Figure IV-7 shows all results for silty clay loams. Figure IV-8 shows Wiebe's results for a fine sandy loam. Keeping in mind the inherent accuracy of the readings, Figures IV-5, IV-6, and IV-7 compare reasonably well with Wiebe's results in Figure IV-8.

This chapter has provided the relationship between soil moisture content and soil electromagnetic properties. The complex dielectric constants versus percent soil moisture curves can be used to predict apparent temperatures for varying moisture contents using the techniques discussed in Chapter III.

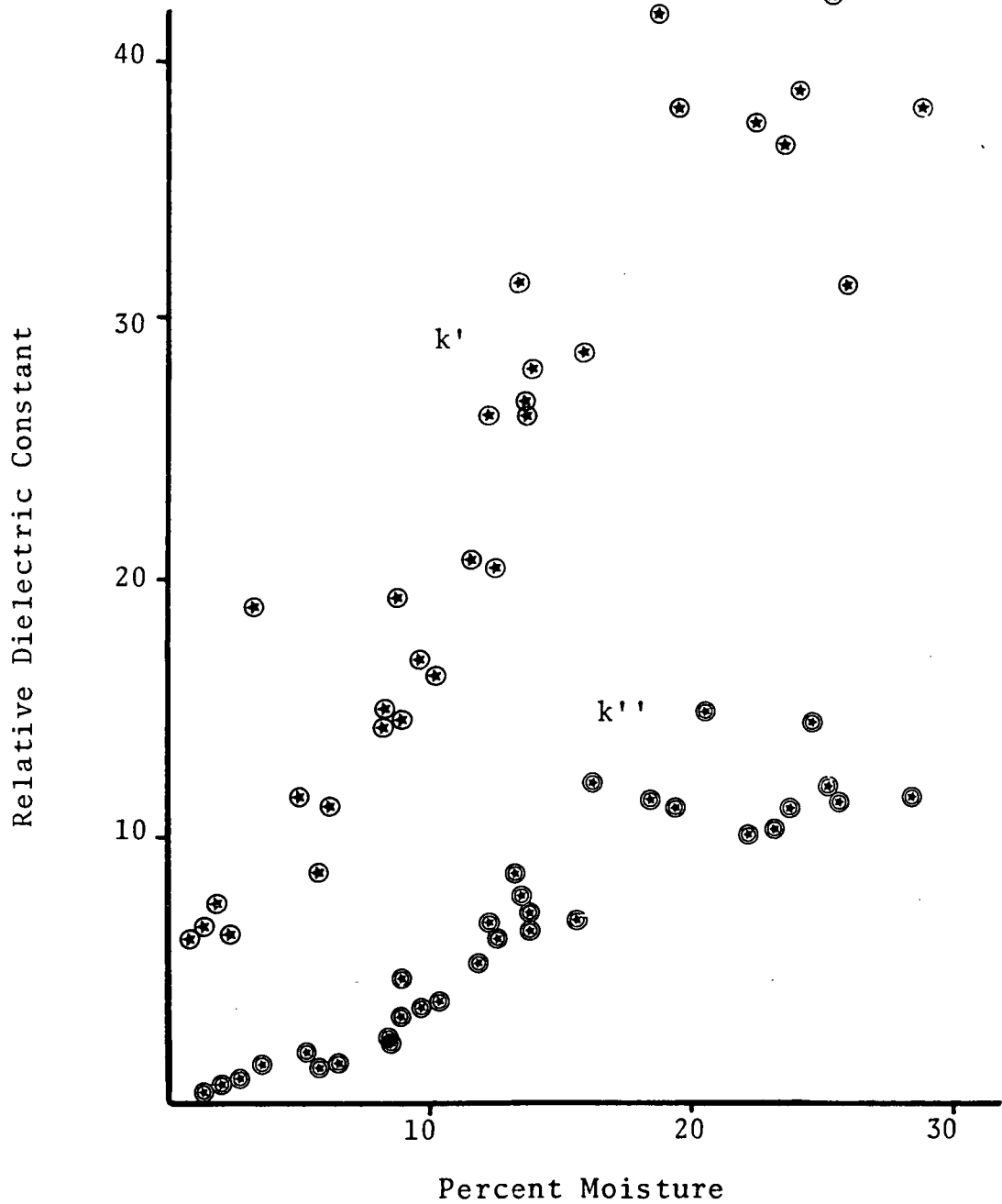


Fig. IV-5. Relative complex dielectric constant for all soils tested.

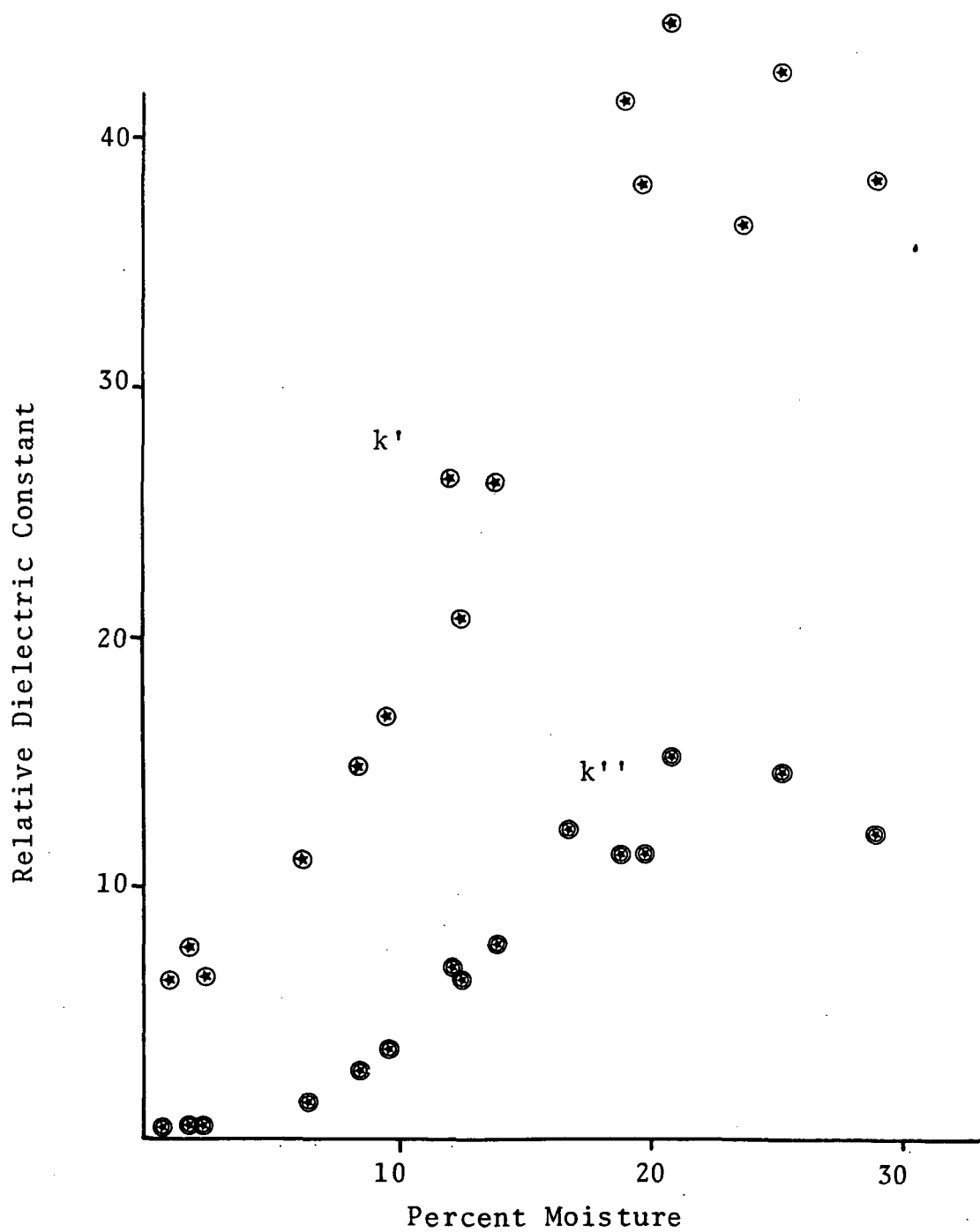


Fig. IV-6. Relative complex constant for silty loam and loamy soils.

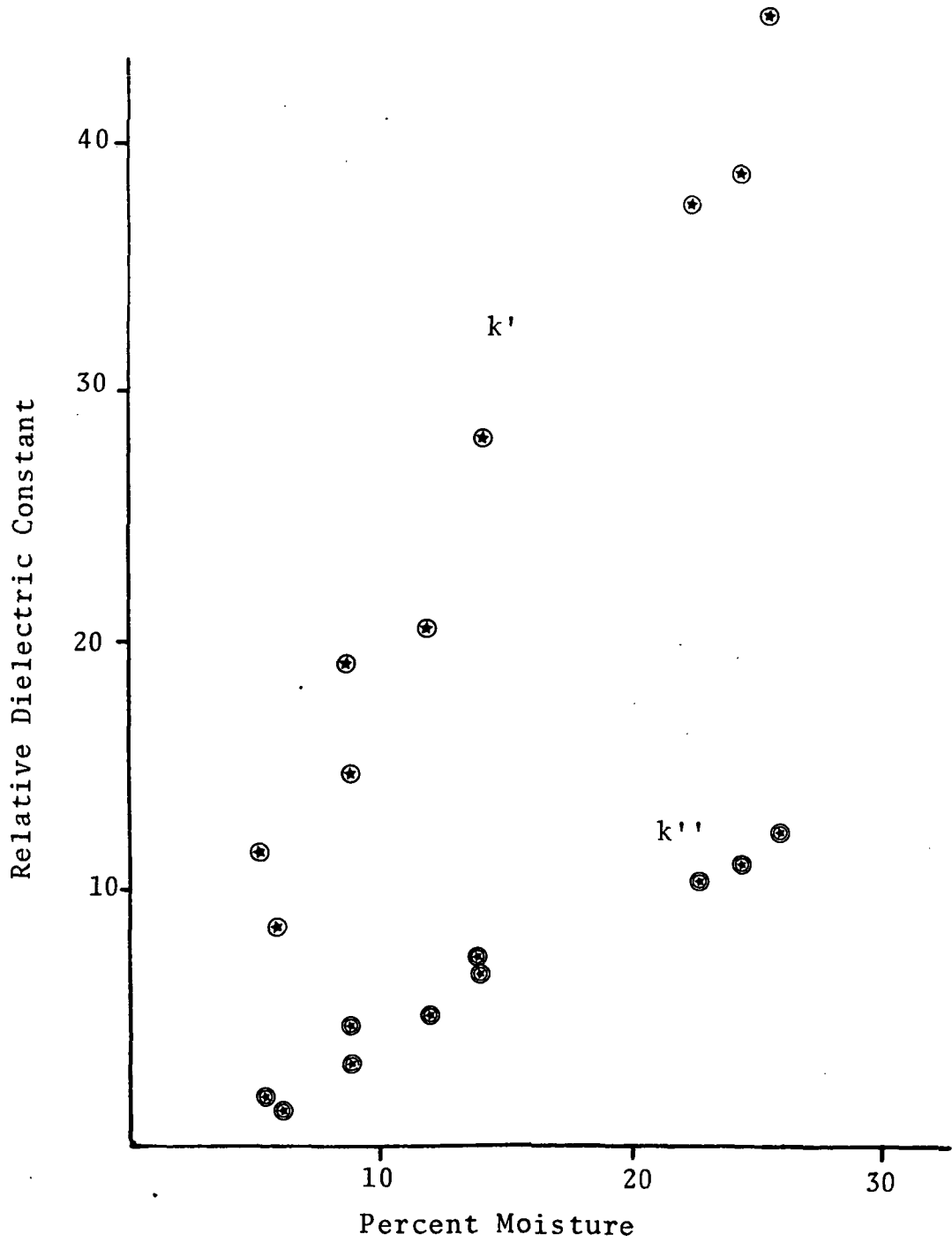


Fig. IV-7. Relative complex dielectric constant for all silty clay loams.

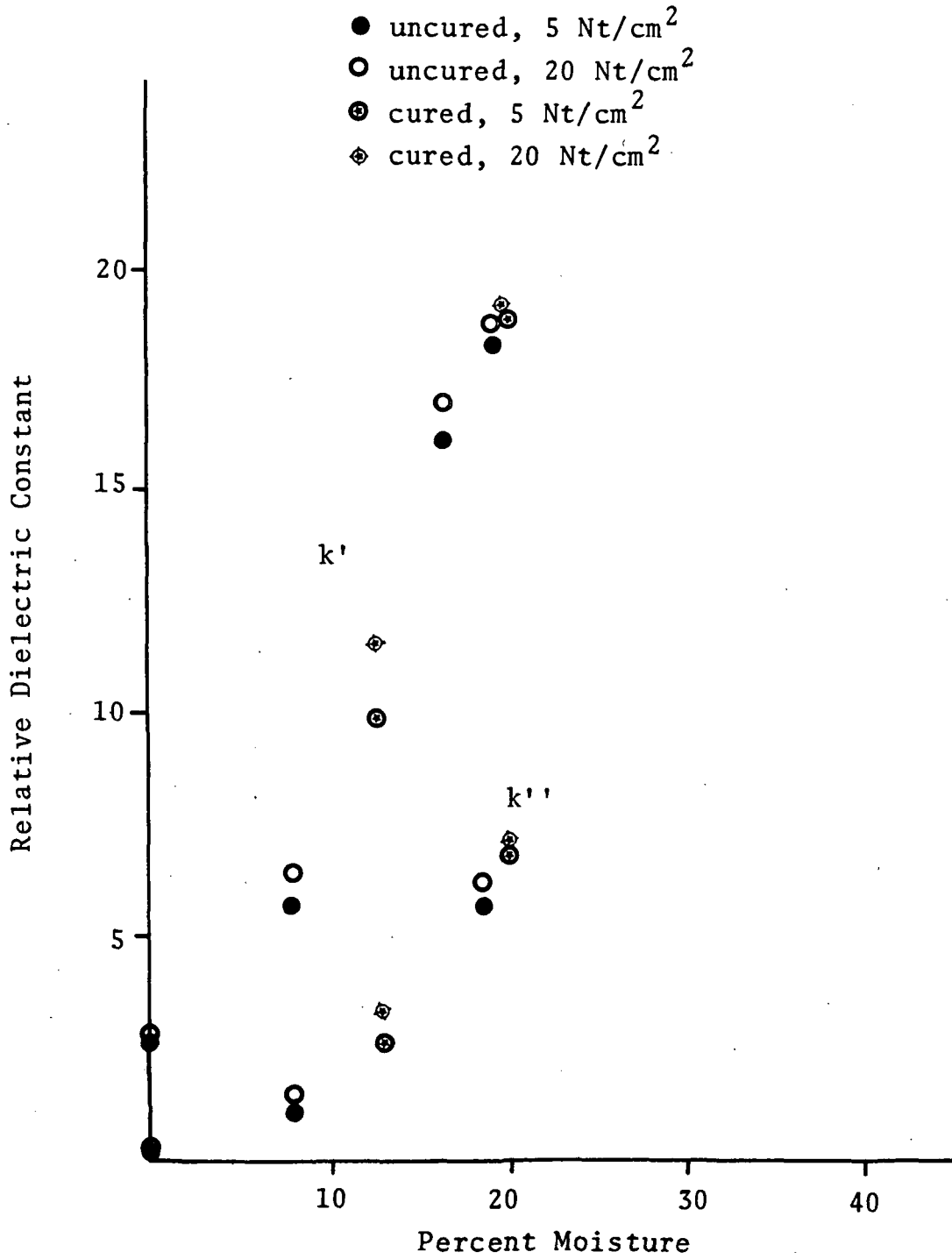


Fig. IV-8. Relative complex dielectric for a fine sandy loam [41].

CHAPTER V

AIRBORNE MEASUREMENTS PROGRAM

An airborne measurements program consisting of two separate test sites was performed with the cooperation of the National Aeronautics and Space Administration, Goddard Space Flight Center. The flights were aimed at observing soil moisture with multi-frequency microwave radiometer. Two test sites were located near Chickasha, Oklahoma and Weslaco, Texas. The objective of the overall airborne program was to provide a set of radiometric measurements with enough reliable supporting ground truth information to facilitate interpretation.

Description of Test Sites

Chickasha

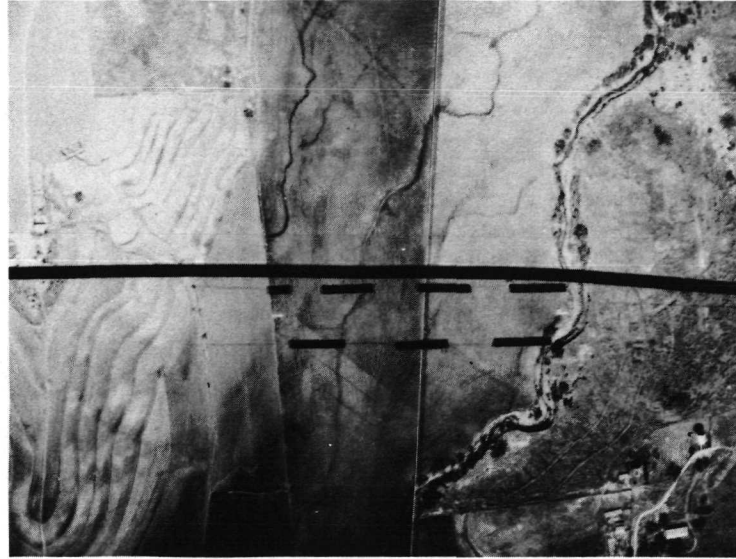
In 1961, the USDA established the Southern Plains Watershed Research Center in Chickasha, Oklahoma to determine the change in downstream runoff, sediment flows, and ground-water levels when flood control measures are applied in the uplands of the Wachita River basin. The research center has continuously monitored the hydrologic characteristics of the area since 1961 in order to evaluate and perfect mathematical modeling of the runoff

characteristics of the river basin. Since 1969 remote sensing techniques have been employed in their research.

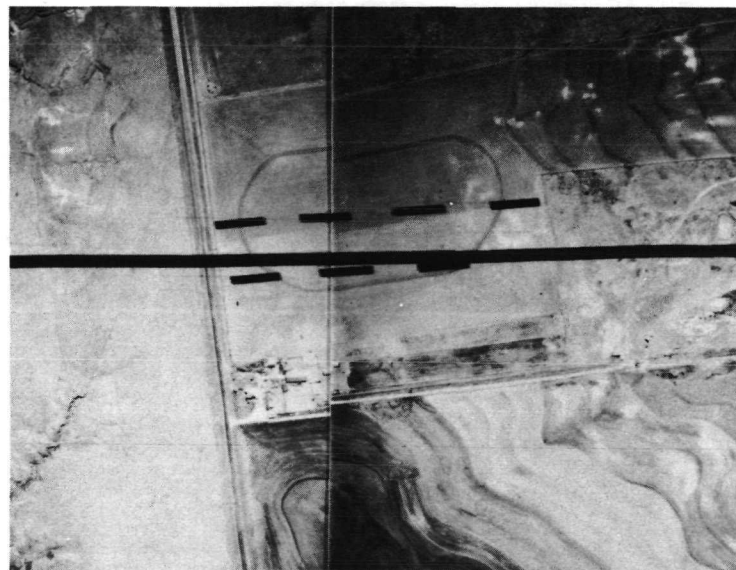
Most of the emphasis in remote sensing at Chickasha has been directed toward surface soil moisture measurements, or indirectly, the rainfall storage capacity of the soil. Two flights of the NP-3A aircraft operated by NASA/Johnson Space Center in 1969 and 1971 have been made.* In addition to soil moisture determination, other objectives of the remote sensing missions have been to measure pond-water quality, to describe geologic sources of sediment, and to develop rapid methods of mapping seepages [19].

The Chickasha overflight consisted of 11 specific test sites numbered A through K comprising two separate flight lines. Figures V-1, V-2 and V-3 show 5 of the Chickasha test sites. The sites vary in length from 200 to 1200 meters. Two predominant soil types exist in the area of the sites, Reinach silt loam and McLain silty clay loam. The complex permittivities of these two soils were measured and appear in Figures IV-5 and IV-6. A vegetation cover of young wheat, which is kept short by periodic grazing of livestock, is present on most of the

*The results of the microwave radiometer investigations are presented in Chapter VI.



(a) Site A

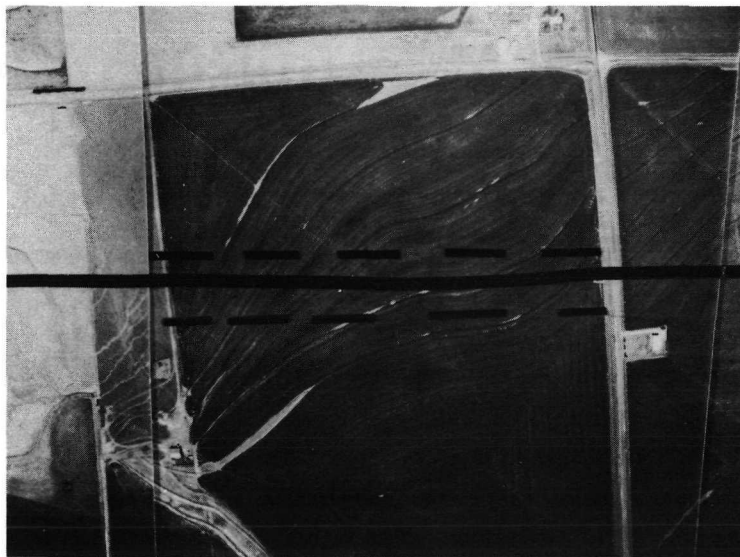


(b) Site B

Fig. V-1. Chickasha test sites



(a) Site G



(b) Site H

Fig. V-2. Chickasha test sites

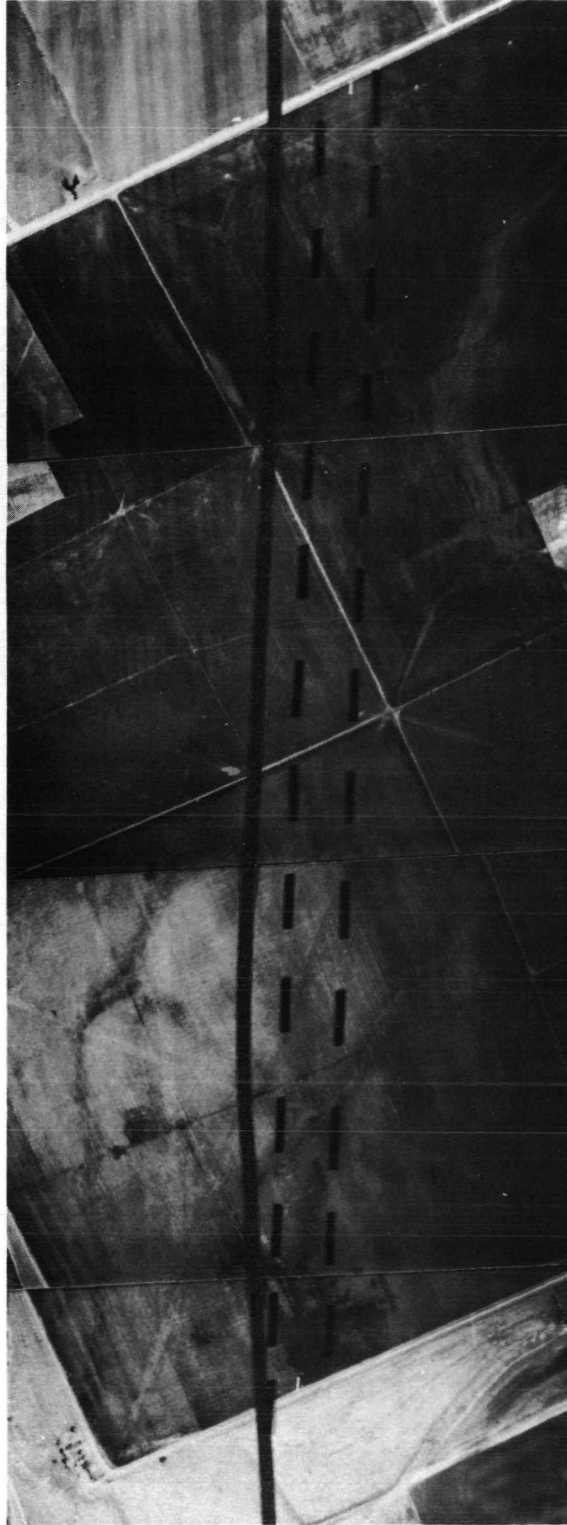


Fig. V-3. Chickasha test site I.

test sites.

The supporting ground measurements for the flight were performed by personnel of the Southern Plains Watershed Research Center. Two soil moisture sampling lines parallel to and 30 meters either side of the flight line were taken at intervals of 30 meters. The rationale of the sampling scheme was to provide compensation if the aircraft were to deviate from the established flight line. Temperatures for the air, the ground, and the vegetation canopy were recorded for each of the 11 sites. When possible, a wheat cutting was taken and a percent moisture determination for the canopy was computed. Figures V-4 through V-6 show ground cover of the fields on the day of the flight, March 14.

The soil sampling procedure consisted of taking a sample from the top 10 cm of surface soil, disregarding the initial 1 cm of the surface because the drying effect of the wind causes a crusty layer which often is not representative of the actual moisture content of the soil. The percent moisture content of the samples were determined according to (IV-1). A histogram showing the distribution of moisture content for the Chickasha samples is given in Figure V-7.



(a) Site A



(b) Site B

Fig. V-4. Ground cover for Chickasha sites



(a) Site C



(b) Site F

Fig. V-5. Ground cover for Chickasha sites



(a) Site G



(b) Site H

Fig. V-6. Ground cover for Chickasha sites

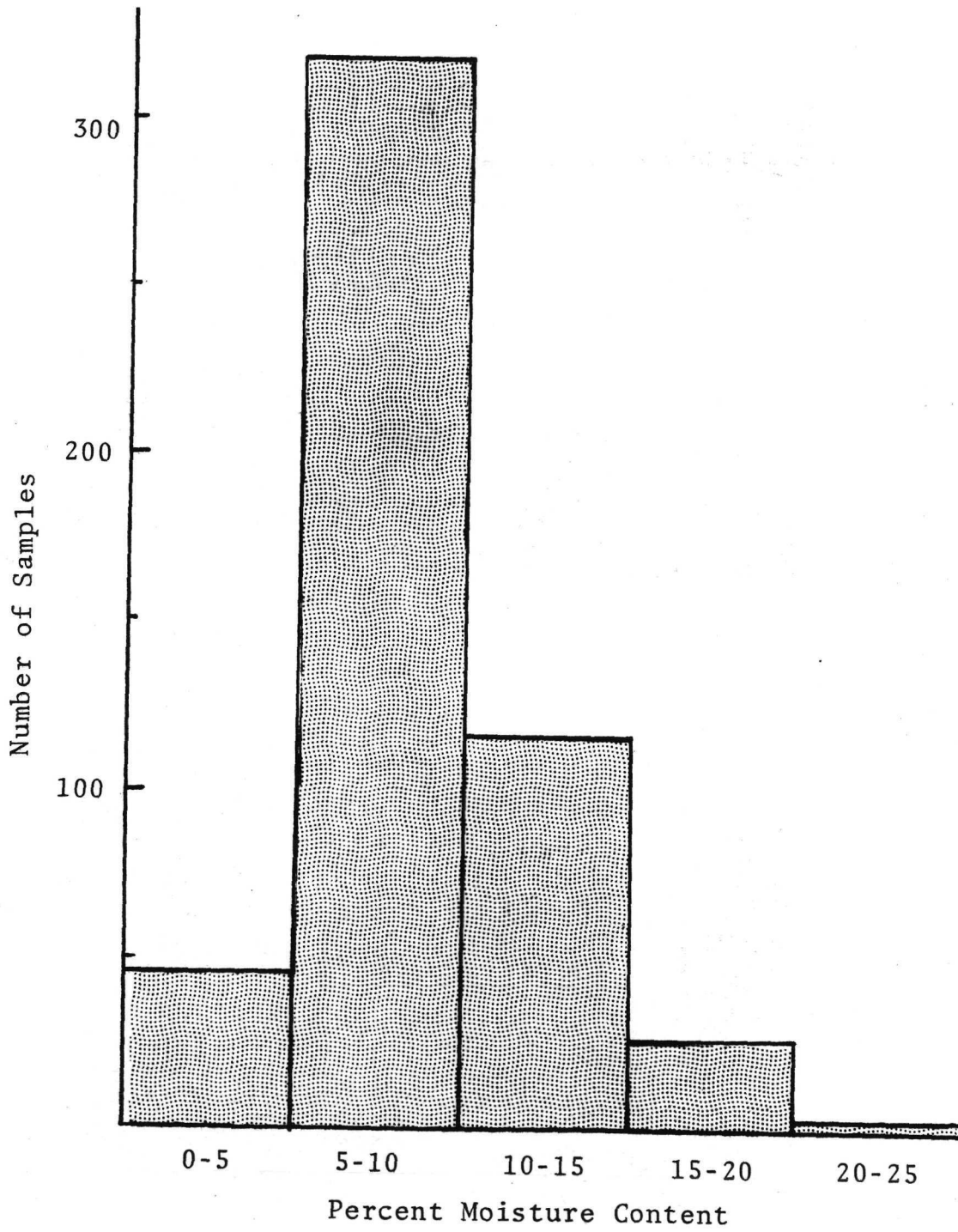


Fig. V-7. Distribution of percent moisture content for Chickasha soil samples

Weslaco

The Rio Grande Valley in South Texas is typically a semi-arid region which relies heavily on irrigation for agriculture. Agriculture is the basis for the economy of the area, and the region is extremely productive, especially in vegetables and citrus fruits. The Weslaco area is an appropriate location for development of sensors to monitor soil moisture because large moisture variations normally exist from one field to another, depending on elapsed time from the most recent irrigation for each field. A histogram depicting the distribution for all soil moisture samples taken from the Weslaco flight line is given in Figure V-8.

The flight line consists of 29 kilometers of agricultural fields running parallel to and just south of highway US 281. Similar research was done by Jean [10] for the same flight line in 1971. The predominant soil type of the area is Harlingen clay which has a clay fraction content of 61.5% by weight and a silt fraction content of 36.97% for the top 27 cm of soil [44]. The fields are approximately 400 by 500 meters, and roughly half of the fields were bare on the day of the flight, March 14. The fields which were vegetated contained corn, onions, tomatoes, sorghum, or cabbage. The bare fields were

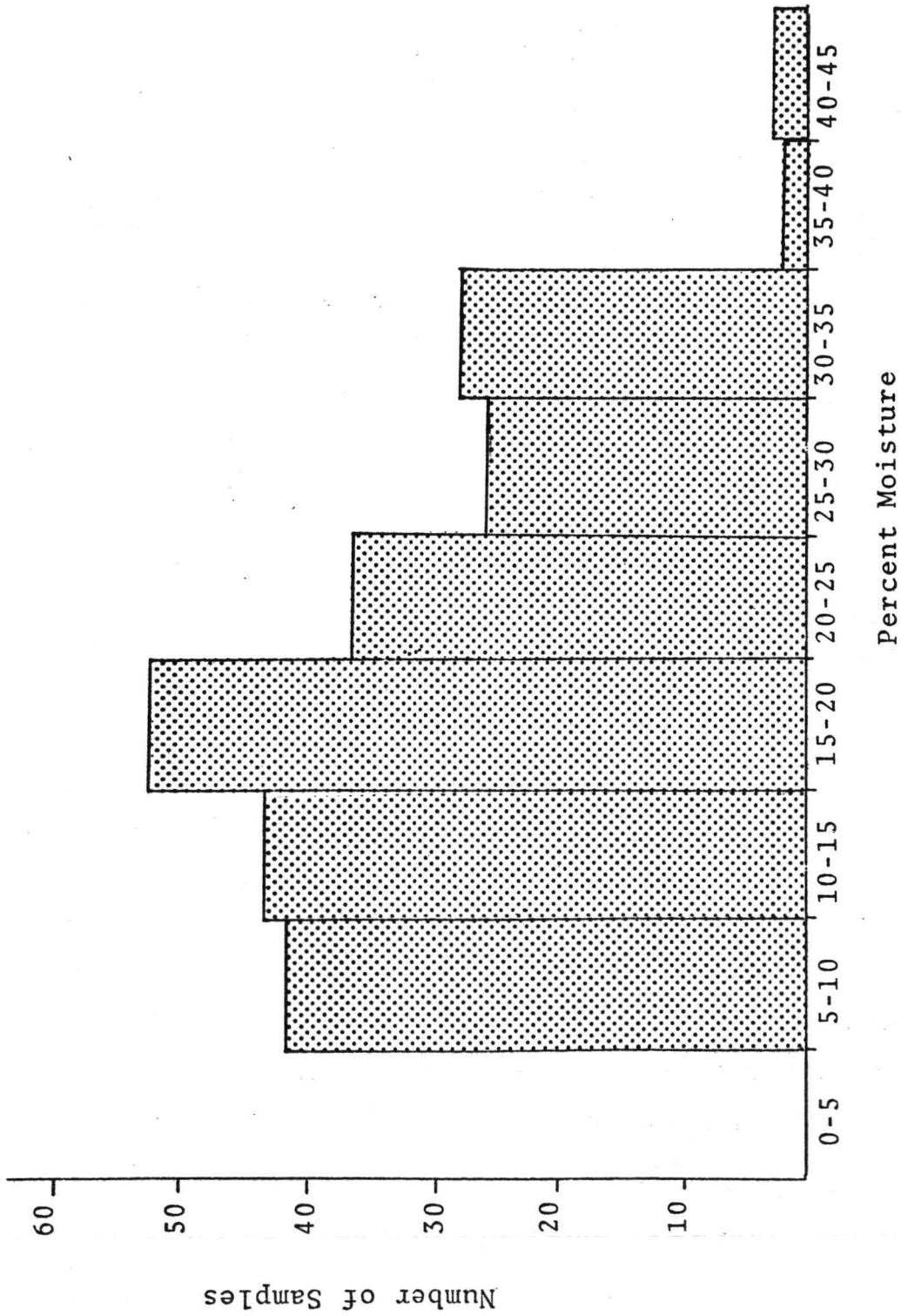


Fig. V-8. Distribution of moisture content for Weslaco soil samples.



(a)



(b)

Fig. V-9. Typical fields along Weslaco flight line.

either furrowed or plowed (see Figure V-9).

The ground truth survey was performed by members of the Remote Sensing Center, Texas A&M University. Only the bare fields were sampled, and the procedure for taking and processing the soil sample was the same as for Chickasha, a 10 cm sample with the top 1 cm disregarded. The center line was determined by moving 200 meters south from US 281 into the field. 3 samples were taken every 100 meters along the flight line, one sample on the center line and samples 75 meters from and on a line perpendicular to the center line, thus forming a grid pattern of samples, again to insure that slight inaccuracies on the part of the aircraft would not cause it to miss the sampling points on the ground with the field of view of the radiometers.

Aircraft Program

The radiometric measurements were made with the Convair 990 aircraft operated by the National Aeronautics and Space Administration, Goddard Space Flight Center, Greenbelt, Maryland. Table V-1 provides a list of the radiometers on board the aircraft. Significant changes were made on the radiometers since Jean [10] reported the results of a mission in 1971. The 4.99 GHz radiometer was modified so that its viewing angle was 38° to the fore

TABLE V-I

RADIOMETER SYSTEMS ON BOARD THE NASA CV-990 AIRCRAFT

MARCH 14, 1972

Frequency (GHz)	Polarization	Look Angle	3 dB Antenna Beamwidth	Sensitivity ¹ (°K)	Bandwidth (MHz)
1.42	V & H	Nadir	15°	0.9	28.4
4.99	V & H	38° fore	5°	2.0	6.0
9.3	-	Zenith	-	-	-
10.69	H	38° aft	6°	-	-
19.35	H	Scanning ²	2.75°	-	400.0
31.4	-	Zenith	-	-	-
37.0	V & H	38° aft	5°	0.5	300.0

¹Based on an integration time of 1 second.

²This radiometer scans 49.3° perpendicular to the flight path in 39 steps of 2.3°.

while the 10.69 and 37.0 GHz radiometers were installed with an aft viewing angle of 38° . All other radiometers retained their configurations from the Spring of 1971, except for the 2.69 GHz radiometer which was removed from the aircraft.

Infrared photography and thermal infrared measurements supported the measurements of the microwave radiometers. The near-infrared photography was taken using a 70 mm Vinton camera with a number 12 filter. The lens had a field of view of 68.5° . A PRT-5 infrared radiometer was used to measure the spatial physical temperatures of the ground along the flight line.

The CV-990 aircraft was requested to fly at a low altitude and velocity in order to obtain as much quality information as possible from the flights. The altitude, velocity, and antenna beamwidth combine to limit cell size resolution as described in Chapter II. The system trade-offs which exist favor increased temperature sensitivity and greater spatial resolution for low altitudes and velocities.

Results of the Flights

The aircraft was originally scheduled to pass over the Weslaco flight line the afternoon of March 13, 1972 and again the morning of March 14. Upon completion

of the passes over Weslaco on the 14th the aircraft was to fly directly to Oklahoma and complete the mission with several passes over the two Chickasha flight lines.

Before the arrival of the CV-990 in Weslaco on March 13, a heavy downpour invalidated the ground truth measurements which had been taken during previous days' sampling operations. Over 4 inches of rain fell on the Weslaco flight line the afternoon of the 13th. Personnel on board the aircraft observed the severe thunderstorm on the weather radar and the airplane turned back before reaching the area. A visual inspection of the Weslaco flight line the morning of March 14 revealed that all the fields were completely saturated from heavy rains and that sampling operations were not possible. The mission sequence was reversed and the Chickasha flight lines were flown the morning of March 14 and the Weslaco line was delayed until the afternoon of the 14th, thus allowing more time for the water not absorbed by the soil to drain.

Three passes over the two flight lines in Oklahoma were made; the first pass was flown at an elevation of 3,077 meters and with a velocity of 250 knots, while the second and third passes were flown at 615 meters elevation with a velocity of 230 knots. The sensors on board the CV-990 experienced a malfunction lasting approximately 4 minutes during the final pass, hence only a small

amount of data for the final pass were available.

The reasoning behind multiple 615 meter passes over the respective Chickasha test sites was to insure that the actual flight of the aircraft corresponded with the ground measurements for a minimum of one pass per site. The more accurate of the low altitude passes was the final pass, which was degraded in part by sensor malfunction; however, a combination of the results provides accurate coverage for nearly all of the 11 test sites in Oklahoma. The 3,077 meter pass included in the flight plan was not readily applicable to this experiment due to the poor spatial resolution and the difficulties in alignment at high altitudes.

Two 615 meter passes were made over the Weslaco flight line. Accurate adherence to the established flight line has little significance since the Weslaco fields were analyzed only with regard to the aerial photography, thermal infrared temperature readings, general characteristics of each field as recorded in the ground operations, and a knowledge that the fields were saturated.

Summary of Airborne Experiment

Perhaps the most important, as well as the most difficult element of any research effort, is the program of the experiments. The airborne experimental program

described here did not conform to anticipated results, however, a usable data set was produced despite the problems encountered.

The Chickasha phase of the experiment encountered problems with sensor malfunction and some flight inaccuracies, but the ground measurements were very thorough and accurate aircraft information was obtained for nearly all the sites. The Weslaco experiment, characterized by the heavy rains prior to the flight, did not produce the expected data sets of radiometer apparent temperatures for a variety of percent moisture contents of the soil; however, with the consistent moisture levels in the fields, the substantial differences in apparent temperatures which occur in the data provide knowledge of other parameters affecting the apparent temperatures.

CHAPTER VI

ANALYSIS OF EXPERIMENTAL DATA

Chapter V described the measurement procedure followed in obtaining airborne microwave radiometer data along selected flight lines in Chickasha, Oklahoma and Weslaco, Texas. The data obtained in the experiment were analyzed to determine the dependence of measured apparent temperature to soil moisture content. The results of the analysis are compared to both previous experimental work and theoretical predictions. The unique features of the Weslaco portion of the airborne experiments gives a basis on which to infer the behavior of the measured apparent temperatures for parameters other than soil moisture content.

The analysis has been divided into three distinct areas. The results of the analysis of the data obtained in Chickasha are given in the first section. The data from the Weslaco experiment are given in the next section, and the combined results from the Chickasha and Weslaco flights are analyzed in the third section.

The data available for analysis was limited due to problems associated with the calibration procedures and problems in the data processing of the initial analog signals. Only the 1.42 GHz (vertical and horizontal), 37.0 GHz (vertical and horizontal), and 19.4 GHz (horizontal)

results were considered in the analysis. The 19.4 GHz radiometer is a scanning type radiometer, however, only the center cell was used in order to view the area along the flight path and to have a constant nadir look angle. The 1.42 GHz and 19.4 GHz radiometer results are considered more meaningful to this study than are the 37.0 GHz results because the 37.0 GHz radiometer had an aft look angle of 38°. The photomosaic of the flight lines revealed that the aircraft heading and the flight path were often different due to crosswinds, hence the viewing area of the 37.0 GHz radiometer did not always coincide with the area along the flight path. In addition, the aircraft altimeter did not function properly, hence deviations in altitude, which affected the coverage of the radiometers with look angles other than nadir, went undetected.

The PRT-5 radiometer results did not correspond with known ground temperature readings for the Chickasha fields, thus the infrared temperature readings were deemed unreliable for the purposes of this study and were omitted from the analysis.

Chickasha Data Analysis

The only data with verified ground measurements obtained from the airborne experiment were the Chickasha data.

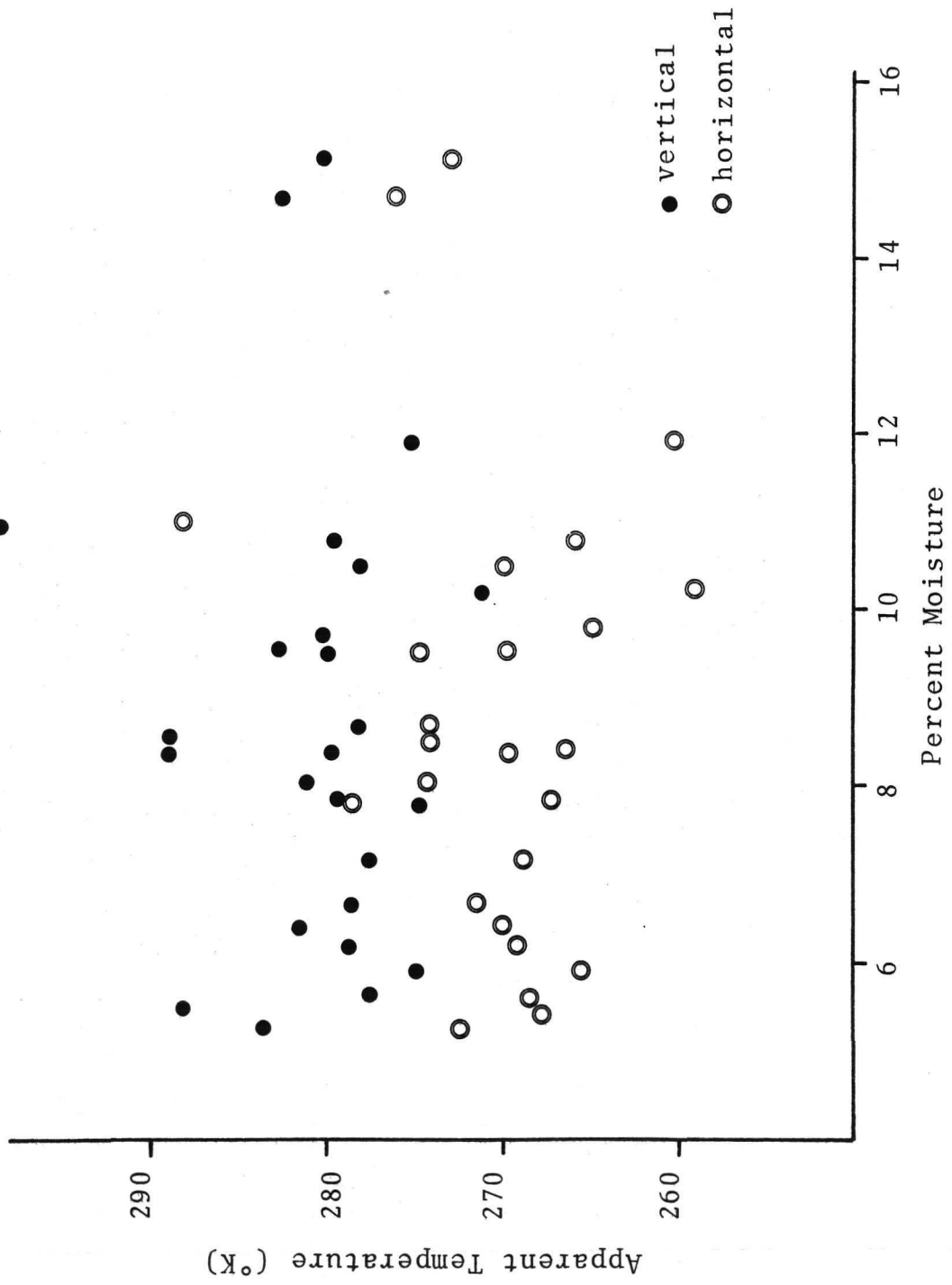


Fig. VI-1. 1.42 GHz radiometer results for sites I, J, and K.

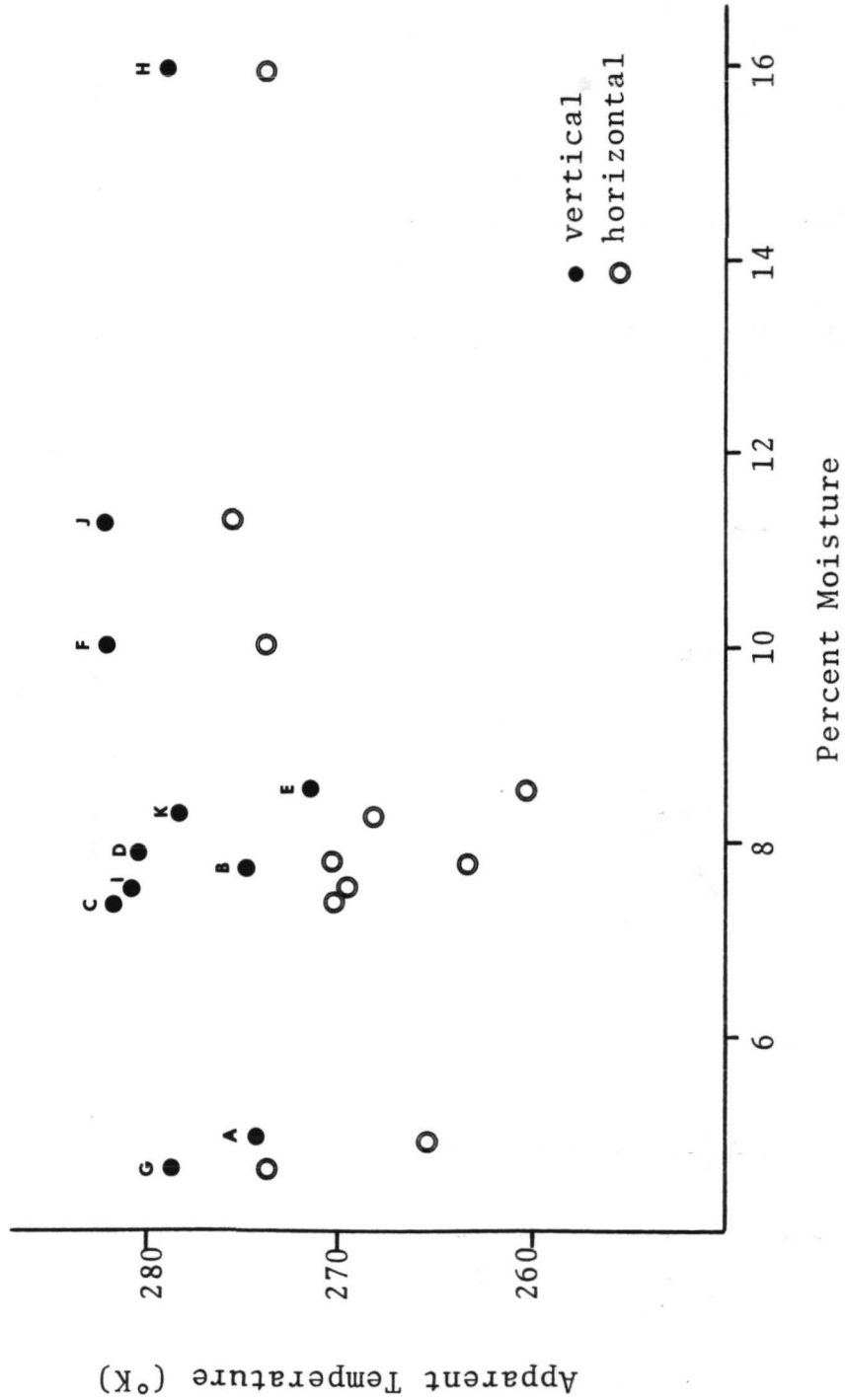


Fig. VI-2. 1.42 GHz radiometer results for Chickasha test sites.

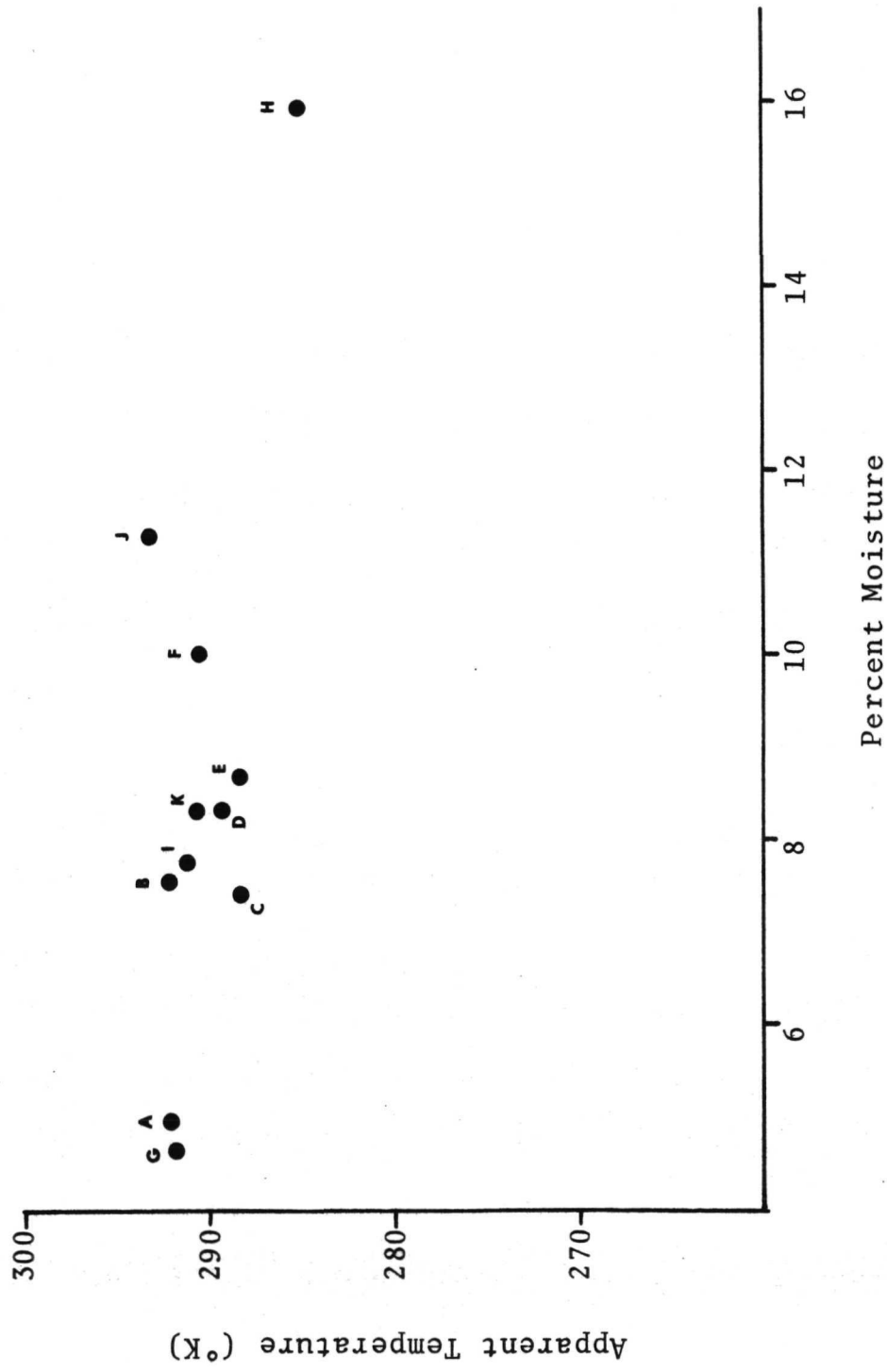


Fig. VI-3. 19.4 GHz radiometer results for Chickasha test sites.

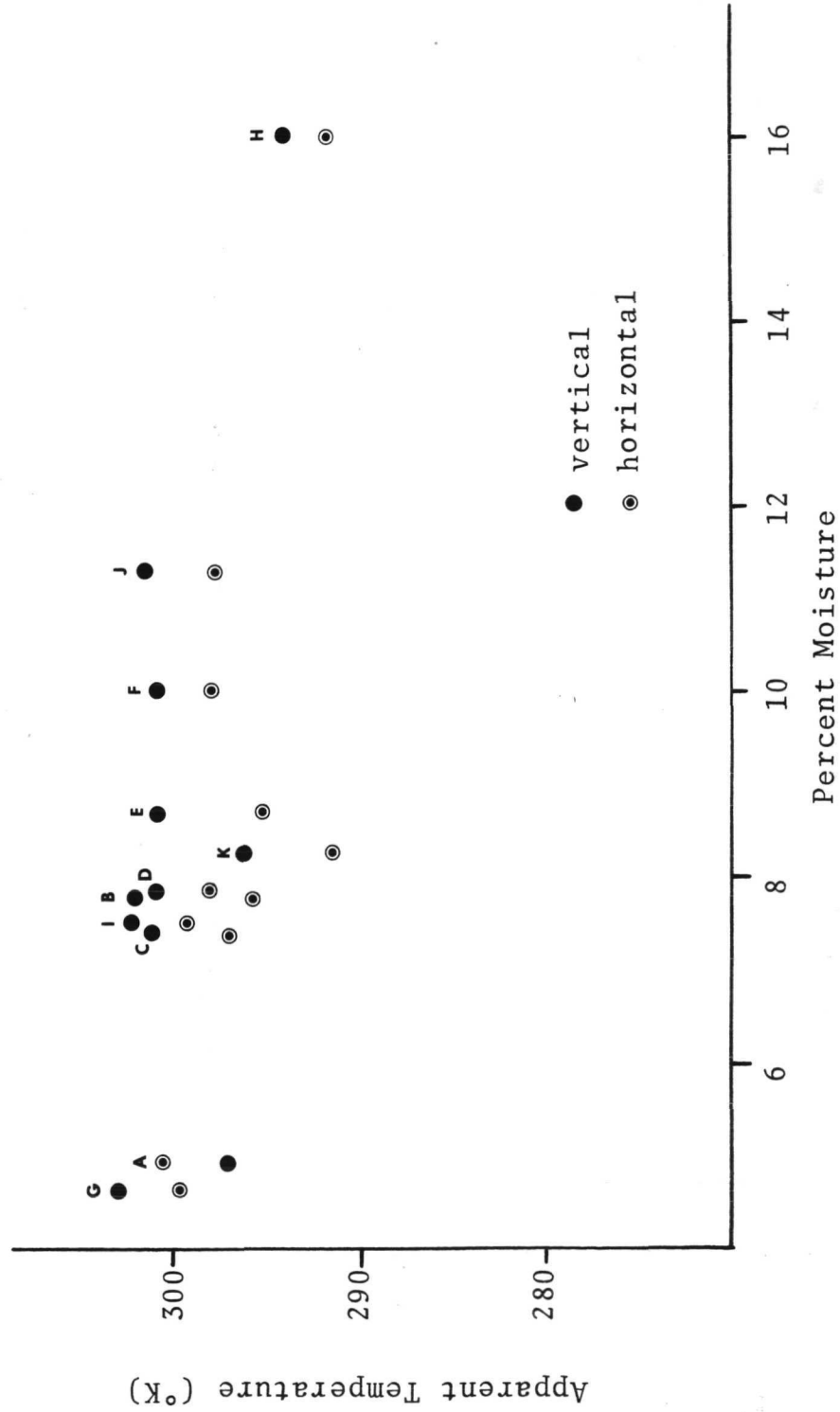


Fig. VI-4. 37.0 GHz radiometer results for

Chickasha test sites.

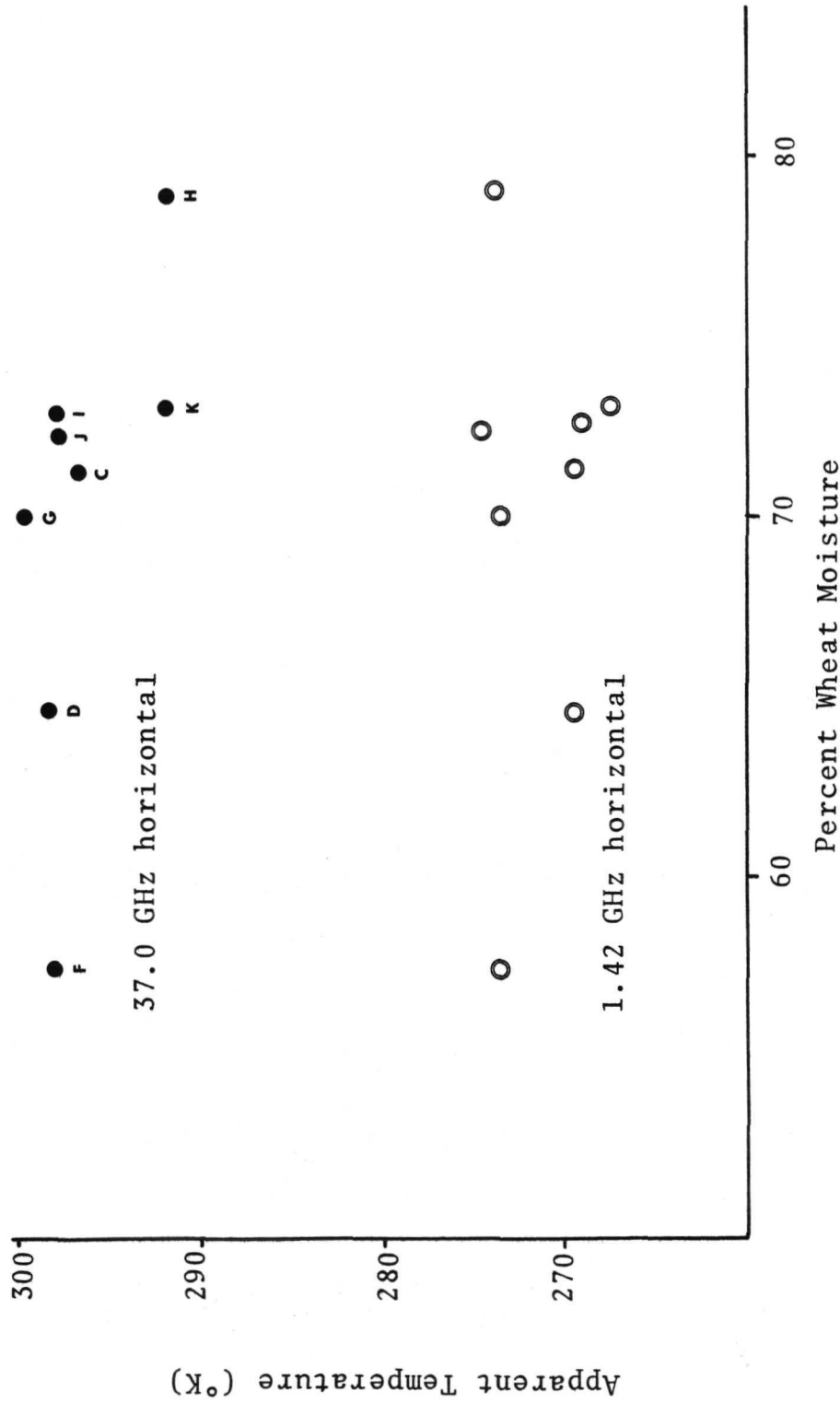


Fig. VI-5. Apparent temperatures versus wheat moisture for Chickasha test sites.

The aircraft flight path corresponded well with the ground measurements. The larger fields, sites I, J, and K (see Figure V-3, p. 69), have a sufficient number of apparent temperature measurements to examine the behavior of percent soil moisture content and apparent temperatures across the sites. The results of the 1.42 GHz vertical and 1.42 GHz horizontal measurements are plotted versus percent soil moisture in Figure VI-1. The apparent temperatures in Figure VI-1 do not show a discernable dependence on soil moisture constant.

Average values for the percent moisture content of the sites were compared to the average values of the measured apparent temperatures for each site. The results of the 1.42 GHz radiometer are plotted in Figure VI-2. Again no dependence of soil moisture and apparent temperature can be observed from the data. Figures VI-3 and VI-4 contain the plotted results of the 19.4 GHz and 37.0 GHz radiometers, respectively, with no apparent dependence with percent soil moisture.

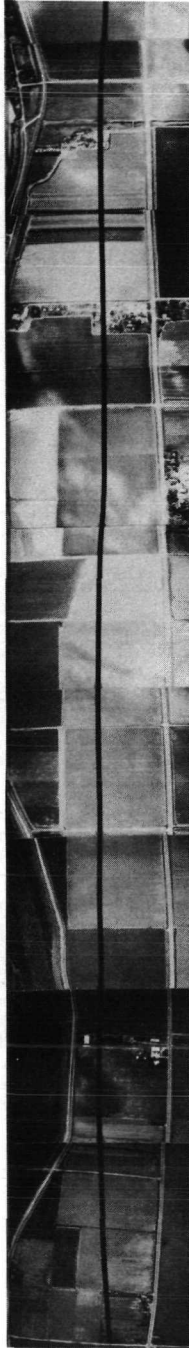
A linear regression was performed for the average values of the five channels of apparent temperature (1.42 GHz vertical and horizontal, and 37.0 GHz vertical and horizontal) with percent moisture as the dependent variable. The regressions confirmed the lack of correlation as observed from the plotted results.

Included in the ground measurements for the Chickasha sites are present moisture determinations of the vegetation covering the sites. The percent moisture of wheat cuttings (wet weight basis) from 10 sites is plotted versus the average measured apparent temperatures for the 1.42 and 37.0 GHz radiometers, horizontal polarization, in Figure VI-5 with no apparent correlation.

Weslaco Data

As reported in Chapter V the Weslaco flight line was completely saturated with water the day of the flight, March 14, as a result of a heavy rainstorm March 13. All fields were estimated to have approximately the same moisture content, about 40-45 percent. This estimation was based on the sampling of freshly irrigated fields in the ground measurement program conducted before the rains [45] and the soil moisture retention curves for Harlingen clay [44]. With a uniform moisture content existing throughout the fields, some conclusions as to the effect of vegetation on measured apparent temperature can be inferred.

Figure VI-6 shows a photo mosaic of a portion of the Weslaco flight line. The computer plot of the apparent temperatures, scaled in time to align with the photomosaic, shows that distinct differences between the vegetated and bare fields exists for all frequencies and polarizations.



WESLACO APPARENT TEMPERATURES--615 METERS--SECOND PASS--WEST END

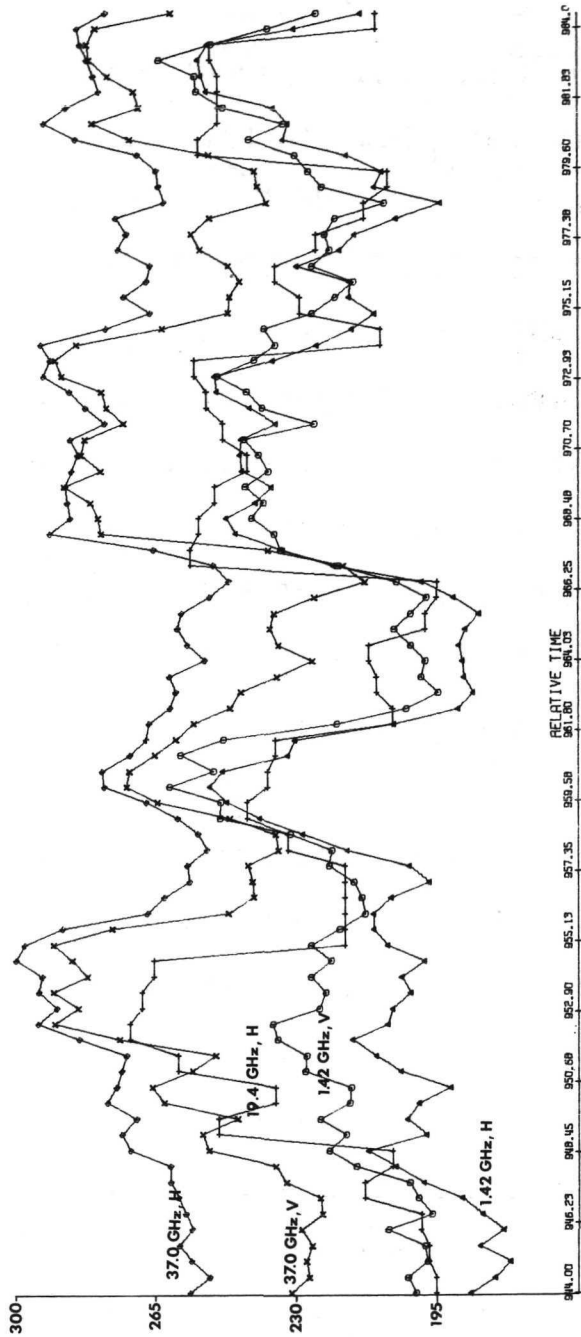


Fig. VI-6. Photomosaic of a portion of the Weslaco flight line with corresponding apparent temperatures.

Combined Analysis of Chickasha
and Weslaco Data

The Chickasha apparent temperature data reported previously were shown to have no discernible dependence with soil moisture. However, the moisture levels in the Chickasha fields were very low (<20%), and investigations by Jean [10] and Schmutge et al. [18] have indicated that measured apparent temperatures did not correlate well with soil moisture for low levels of moisture.

The Weslaco fields were estimated to be completely saturated as a result of heavy rains, and all fields were thought to have uniform soil moisture content. An estimate of the range of moisture for the saturated Harlingen clay soil was made from two sources. Freshly irrigated fields were sampled during the ground measurement program. The resulting soil moisture determinations indicated the range of soil moisture to be around 40-45% [45]. The 40-45% soil moisture range agrees with extrapolated results from known moisture retention curves for Harlingen clay [44].

With estimates for the moisture content of the Weslaco soils a comparison of the data for the Chickasha and Weslaco flight lines was possible. The discrete moisture content of the Weslaco soil was assumed to be midway between 40 and 45% for purposes of analysis. Figures VI-7 and VI-8 show the data from the 1.42 GHz radiometer

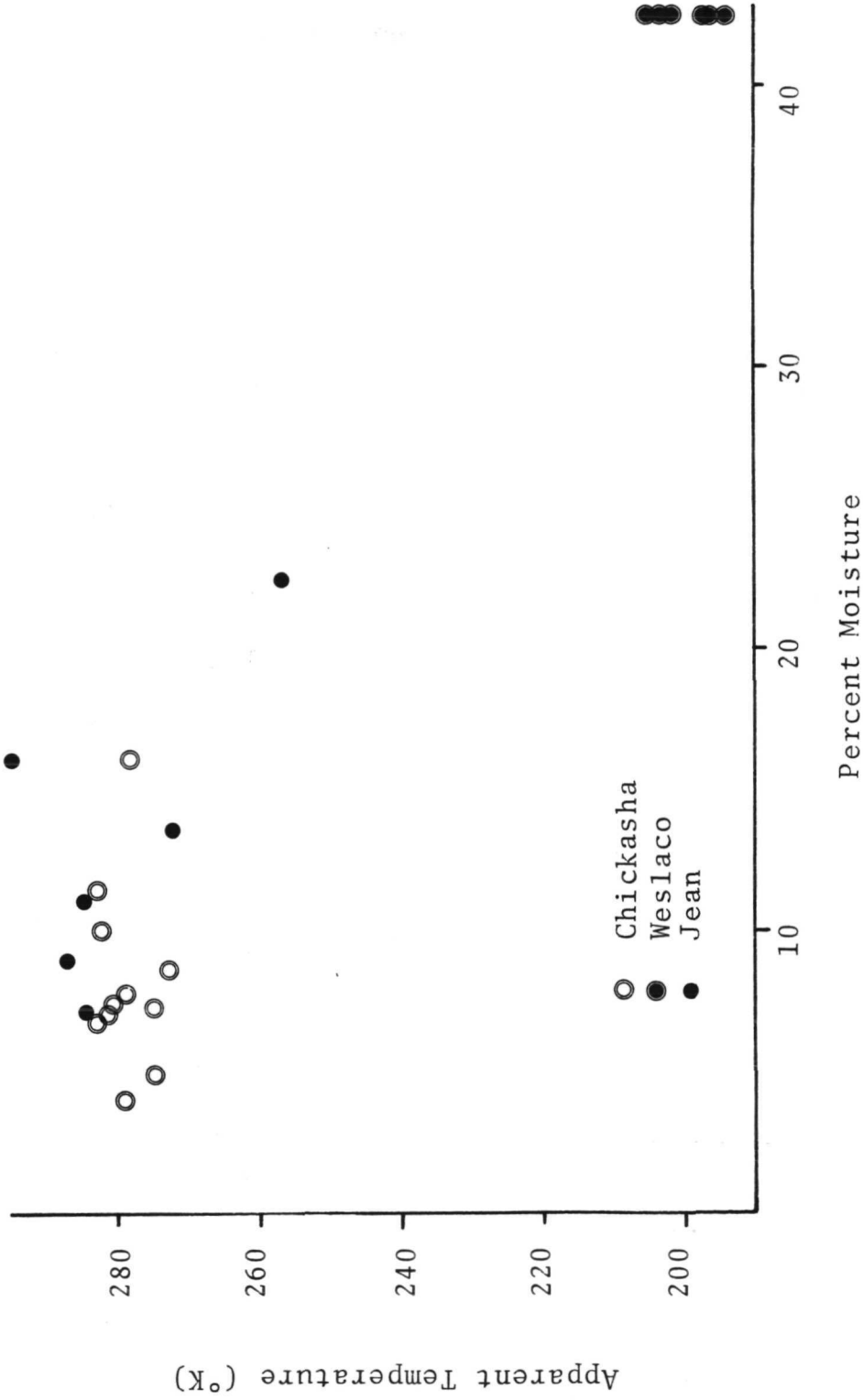


Fig. VI-7. Combined results of the 1.42 GHz radiometer, vertical polarization.

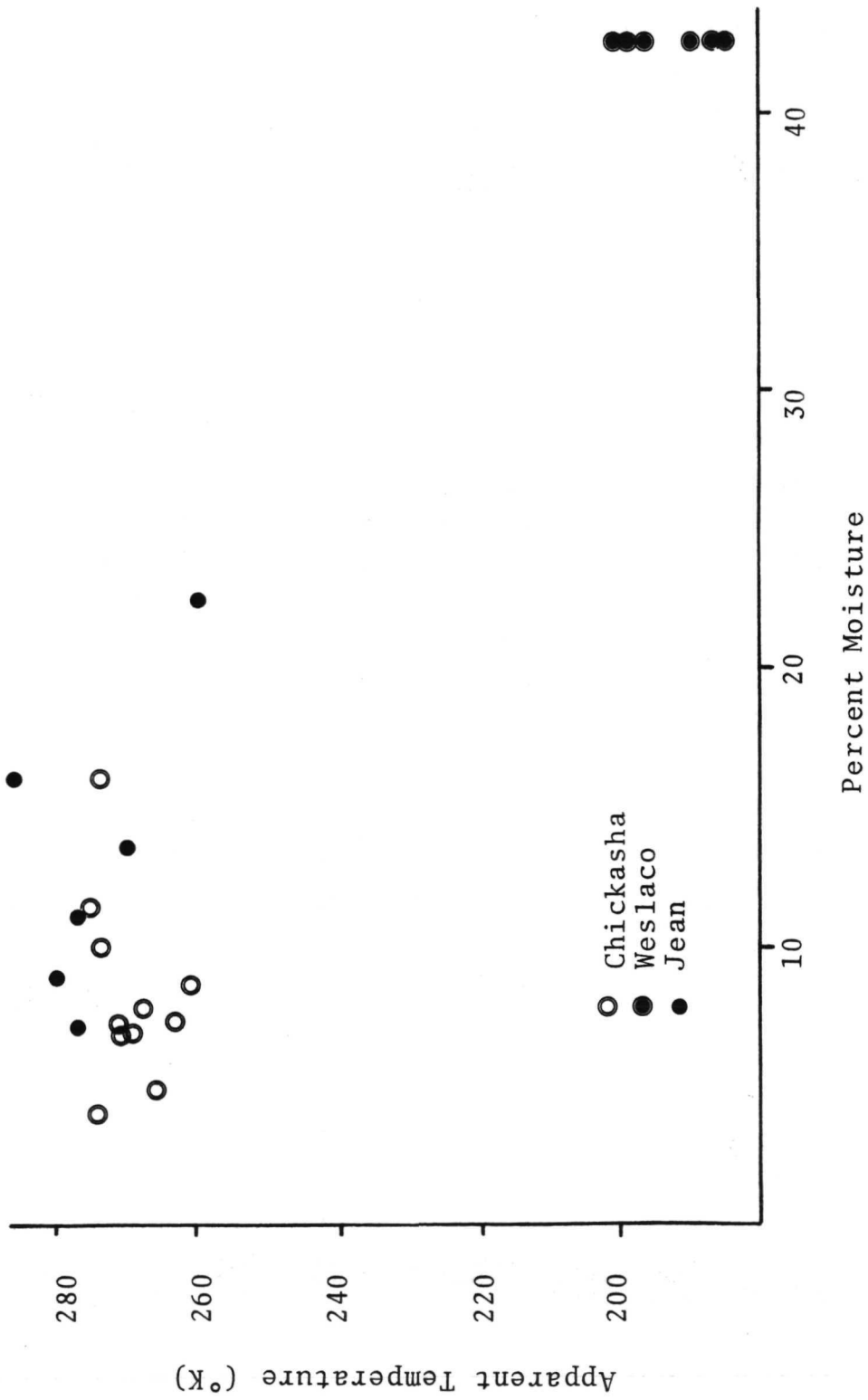


Fig. VI-8. Combined results of the 1.42 GHz radiometer, horizontal polarization.

plotted as a function of soil moisture for the combined results of the Chickasha and Weslaco data sets. Included in the plots are results given by Jean [10]. The comparison of the data shows a definite dependence of measured apparent temperature and soil moisture content.

Optimum linear regression analysis was performed on the five channels of data from the radiometers with soil moisture as the dependent variable. The Hocking-La Motte-Leslie method described by White [46] was used for the regressions. Two regressions were performed. The first regression used average values of data taken from the bare or nearly bare fields of Chickasha and Weslaco. The five channels of data correlated inversely with percent soil moisture as indicated by the negative correlation coefficients shown in Table VI-I. The correlation coefficients were obtained in the same manner as those described by Jean [10]. The optimum regression for a single independent variable indicated that the 1.42 GHz system, vertical polarization, gave the average variation of apparent temperature with moisture content as $-2.15^{\circ}\text{C}/\text{percent soil moisture}$. This value agrees with the average apparent temperature variations given by Jean et al. [16] of $-2.26^{\circ}\text{C}/\text{percent moisture}$ for the same radiometer. Schmutge et al. [18] reported an average apparent temperature variation of $-2^{\circ}\text{C}/\text{percent soil moisture}$.

TABLE VI-I

CORRELATION OF APPARENT TEMPERATURES AND
SOIL MOISTURE CONTENTBare Fields

<u>Data Set</u>	<u>Correlation Coefficient</u>
1.42 V	-0.991
1.42 H	-0.981
19.4 H	-0.975
37.0 V	-0.958
37.0 H	-0.966

Vegetated Fields

<u>Data Set</u>	<u>Correlation Coefficient</u>
1.42 V	-0.915
1.42 H	-0.913
19.4 H	-0.962
37.0 V	-0.743
37.0 H	-0.816

Richerson [15] predicted the theoretical behavior of apparent temperature variations at 31.4 GHz as -1.5 and -1.9°C/percent moisture for the vertical and horizontal polarizations, respectively, for a smooth sandy surface. His results along with the previous experimental results compare reasonably well with the results of the combined analysis of Chickasha and Weslaco data presented.

Summary of Data Analysis

The Chickasha data sets are the only verified data presented, however, the low values of moisture content did not correlate with measured apparent temperatures. With the assumption that the moisture content for the rain soaked Weslaco fields was uniformly consistent midway between 40 and 45%, correlation of apparent temperature with soil moisture content was established.

The results of the combined analysis agrees well with previous studies by Jean et al. [16] and Schmugge et al. [18]. The fact that the Chickasha results alone did not correlate with percent soil moisture content supports the observation made by Schmugge et al. [18] that low values of soil moisture did not correlate well with apparent temperature.

It is obvious from the Weslaco data that vegetation effects can be a large factor in the measured apparent

temperature, and more study needs to be allocated to describe this effect.

CHAPTER VII

CONCLUSIONS AND RECOMMENDATIONS

The development of a remote sensor system to monitor soil moisture content has been proposed for applications in hydrology and agriculture. Of the sensors under investigation, the microwave sensors appear to have inherent advantages over shorter wavelength sensors because of their deeper penetration into the soil and their relative immunity to atmospheric effects.

Airborne microwave radiometer measurements were made over selected flight lines in Chickasha, Oklahoma and Weslaco, Texas. Extensive ground measurements of soil moisture were made in support of the aircraft mission over the two locations. In addition, laboratory determination of the complex permittivities of soil samples taken from the flight lines were made with varying moisture contents.

The data were analyzed to determine the degree of correlation between measured apparent temperatures and soil moisture content. The Chickasha fields were fairly dry (<20° moisture content) and no correlation of apparent temperature with soil moisture existed for the Chickasha data. A heavy rain preceding the Weslaco flight invalidated the ground soil moisture measurements. However, an assumed value of the soil moisture content of the Weslaco fields

was derived from known moisture retention curves for the soil type. The combined results of the Chickasha and Weslaco experiments using the derived soil moisture value yielded a high degree of correlation of apparent temperature and soil moisture. Regression analysis indicated a $-2.15^{\circ}\text{C}/\text{percent}$ moisture variation in apparent temperature for the 1.42 GHz radiometer, vertical polarization, for bare or nearly bare fields, which compares favorably with the results reported by Jean [10]. The center cell of the 19.4 GHz, horizontal, polarization, had an average variation in apparent temperature of $-1.5^{\circ}\text{C}/\text{percent}$ moisture when observing vegetated fields.

The Weslaco data revealed large differences in apparent temperatures for bare and vegetated fields.

The results of the airborne radiometer experiment are encouraging and justify continued research in developing reliable techniques for monitoring soil moisture content. It is recommended that a series of ground based radiometric measurements be made for controlled test surfaces. These measurements should include multiple-frequency, multiple polarization radiometers operated at several look angles. The surfaces should include a wide range of roughness conditions and should be monitored under bare and vegetated conditions. The basic radiative phenomena for standard surface roughness and vegetation need to be examined with

an emphasis on experimental measurements. The dielectric measurements given in this report need to be expanded to include other frequencies of interest. The dielectric behavior of soils with low moisture contents needs to be firmly established. Future airborne experiments should be conducted over the Weslaco flight line because of the wide range of moisture levels at any point in time among the fields. The results from the NASA PMIS radiometer and the radar scatterometers systems should be analyzed to determine the potential for monitoring soil moisture separately or in conjunction with each other.

REFERENCES

- [1] R. H. Dicke, "The Measurement of Thermal Radiation at Microwave Frequencies," The Review of Scientific Instruments, vol. 17, no. 7, July 1946.
- [2] J. P. Hollinger, "Remote Passive Microwave Sensing of the Ocean Surface," Proceedings of the Seventh International Symposium on Remote Sensing of Environment, University of Michigan, Ann Arbor, Michigan, May 1971.
- [3] K. W. Gray, et al., "Microwave Measurement of Thermal Emission from the Sea," Proceedings of the Seventh International Symposium on Remote Sensing of Environment, University of Michigan, Ann Arbor, Michigan, May 1971.
- [4] J. F. Paris, "Microwave Radiometry and Its Application to Marine Meteorology and Oceanography," Reference No. 69-1T, Department of Oceanography, Texas A&M University, College Station, Texas, January 1969.
- [5] J. F. Paris, "Transfer of Thermal Microwaves in the Atmosphere," Ph.D. Dissertation, Texas A&M University, College Station, Texas, May 1971.
- [6] E. Weger, "Apparent Sky Temperatures in the Microwave Region," Journal of Meteorology, vol. 17, April 1960, pp. 159-165.
- [7] A. R. Edison, "Calculated Cloud Contributions to Sky Temperatures at Millimeter-Wave Frequencies," National Bureau of Standards Report 9138, U.S. Department of Commerce, Boulder Laboratories, Boulder, Colorado, February 1966.
- [8] _____, Microwaves, Rochelle Park, New Jersey: Hayden Publishing Company, Inc., vol. 11, no. 11, 1972, pp. 10-16.
- [9] J. C. Aukland and W. H. Conway, "Detection of Oil Slick Pollution on Water Surfaces with Microwave Radiometer Systems," Proceedings of the Sixth Symposium on Remote Sensing of Environment, University of Michigan, Ann Arbor, Michigan, October 1969.

- [10] B. R. Jean, "Selected Applications of Microwave Radiometric Techniques," Master's Thesis, Texas A&M University, College Station, Texas, August 1971.
- [11] P. Gloersen, T. Wilheit, and T. Schmugge, "Microwave Emission Measurements of Sea Surface Roughness, Soil Moisture, and Sea Ice Structure," Presented at NASA-Earth Resources Review, Houston, Texas, January 1972.
- [12] J. M. Kennedy and A. T. Edgerton, "Microwave Radiometric Sensing of Soils and Sediment," American Geophysical Union 48th Annual Meeting, April 1967.
- [13] C. C. Mason, "Detecting Soil Moisture Content with Remote and Contact Temperature Sensors," National Aeronautics and Space Administration, Manned Spacecraft Center, Houston, Texas, October 1969.
- [14] A. E. Basharinov and A. M. Shutko, "The Microwave Radiometric Measurements of Soil Moisture," Institute of Radio Engineering and Electronics of the Academy of Sciences of the USSR, 1970.
- [15] J. A. Richerson, "An Experimental Evaluation of a Theoretical Model of the Microwave Emission of a Natural Surface," Master's Thesis, Texas A&M University, College Station, Texas, August 1971.
- [16] B. R. Jean, C. L. Kroll, J. A. Richerson, J. W. Rouse, Jr., T. G. Sibley, and M. L. Wiebe, "Microwave Radiometer Measurements of Soil Moisture," Technical Report RSC-32, Remote Sensing Center, Texas A&M University, College Station, Texas, October 1972.
- [17] G. Poe, A. Stogryn, and A. T. Edgerton, "Determination of Soil Moisture Content Using Microwave Radiometry," Summary Report 1684R-2, Aerojet-General Corporation, El Monte, California, February 1971.
- [18] T. Schmugge, P. Gloersen, and T. Wilheit, "Remote Sensing of Soil Moisture with Microwave Radiometers," Goddard Space Flight Center, Greenbelt, Maryland, 1972.
- [19] B. J. Blanchard, "Measurements from Aircraft to Characterize Watershed," Presented at NASA - Earth Resources Review, Houston, Texas, January 1972.

- [20] E. H. Stockhoff and R. T. Frost, "Polarization of Light Scattered From Moist Soils," Proceedings of the Seventh International Symposium on Remote Sensing of Environment, University of Michigan, Ann Arbor, Michigan, May 1971.
- [21] J. W. Rouse, Jr., "On the Effect of Moisture Variations on Radar Backscatter from Rough Soil Surfaces," Technical Memorandum RSC-52, Remote Sensing Center, Texas A&M University, College Station, Texas, July 1972.
- [22] R. K. Moore, F. Dickey, C. King, and J. Holtzman, "Moisture Dependency of Radar Backscatter from Irrigated and Non-Irrigated Fields at 400 MHz and 13.3 GHz," Technical Report, University of Kansas, Lawrence, Kansas, 1972.
- [23] H. Werner and F. Schmer, "Application of Remote Sensing Techniques to Cropland and Rangeland Soil Water Inventory," Technical Report RS1-72-16, Remote Sensing Institute, South Dakota State University, Brookings, South Dakota, December 1972.
- [24] M. Planck, The Theory of Heat Radiation, New York: Dover Publications, 1959.
- [25] R. L. Riegler, "Microwave Radiometric Temperatures of Terrain," Report 1903-2, The Ohio State University Research Foundation, Columbus, Ohio, June 1966.
- [26] E. Schanda, "Graphs for Radiometer Applications," Reprint from Elektronica en Telecommunicatie no. 4, April 1971.
- [27] W. H. Peake and T. L. Oliver, "The Response of Terrestrial Surfaces at Microwave Frequencies," Technical Report AFAL-TR-70-301, The Ohio State University Electro Science Laboratory, Columbus, Ohio, May 1971.
- [28] W. H. Peake, "Interaction of Electromagnetic Waves with Some Natural Surfaces," IRE Transactions on Antennas and Propagation, December 1959, pp. 324-329.
- [29] W. H. Peake and S. N. C. Chen, "Apparent Temperatures of Smooth and Rough Terrain," IRE Transactions on Antennas and Propagation, November 1961, pp. 567-572.

- [30] A. P. Stogryn, "The Apparent Temperature of the Sea at Microwave Frequencies," IEEE Transactions on Antennas and Propagation, vol. AP-15, no. 2, March 1967, pp. 278-286.
- [31] F. T. Ulaby, A. K. Fung, and S. Wu, "The Apparent Temperature and Emissivity of Natural Surfaces at Microwave Frequencies," Technical Report 133-12, Center for Research Inc., Engineering Science Division, The University of Kansas, Lawrence, Kansas, March 1970.
- [32] L. F. Johnson, "On the Performance of Infrared Sensors in Earth Observations," Master's Thesis, Texas A&M University, College Station, Texas, August 1972.
- [33] G. Ruck, D. Barrick, W. Stuart, and C. Krichbaum, Radar Cross Section Handbook, New York: Plenum Press, 1970.
- [34] W. H. Peake, "Theory of Radar Return From Terrain," Antenna Laboratory, The Ohio State University, Columbus, Ohio, 1959.
- [35] T. G. Sibley, Private Communication, May 1973.
- [36] H. Kohnke, Soil Physics, New York: McGraw-Hill Book Company, 1968.
- [37] P. Hillel, Soil and Water, Physical Principles and Processes, New York: Academic Press, 1971.
- [38] P. Hertel, A. W. Straiton and C. W. Tolbert, "Dielectric Constant Measurements at 8.6 Millimeter Wavelength," Electrical Engineering Research Laboratory Report No. 65, The University of Texas, Austin, Texas, March 1953.
- [39] J. R. Lundien, "Terrain Analysis by Electromagnetic Means," U.S. Army Engineer Waterways Experiment Station Technical Report No. 3-693, 1971.
- [40] M. L. Wiebe, "Various Techniques of Dielectric Constant Measurement as Applied to the Relative Dielectric Constant of Sand as a Function of Moisture Constant," Technical Memorandum RSC-22, Remote Sensing Center, Texas A&M University, College Station, Texas, April 1971.

- [41] M. L. Wiebe, "Laboratory Measurement of the Complex Dielectric Constant of Soils," Technical Report RSC-23, Remote Sensing Center, Texas A&M University, College Station, Texas, October 1971.
- [42] R. S. Vickers and G. C. Rose, "The Use of Complex Dielectric Constant as a Diagnostic Tool for the Remote Sensing of Terrestrial Materials," AF CRL-71-0438, Department of Electrical Engineering, Colorado State University, Fort Collins, Colorado, August 1971.
- [43] S. Ramo, J. Whinnery and T. Van Puzer, Fields and Waves in Communication Electronics, New York: John Wiley and Sons, 1965.
- [44] M. D. Heilman, J. R. Thomas, P. L. Carter, and C. M. Thompson, "Chemical, Physical, and Mineralogical Characteristics of Eight Irrigated Soils of the Lower Rio Grande Valley of Texas," SWC Research Report 382, Soil and Water Conservation Research Division, USDA, Weslaco, Texas, December 1966.
- [45] C. L. Kroll, "Weslaco Ground Truth Survey in Support of NASA/GSFC CV-990 Aircraft," Technical Memorandum RSC-46, Remote Sensing Center, Texas A&M University, College Station, Texas, June 1972.
- [46] P. E. White, "Water Quality Parameter Measurement Using Spectral Signatures," Technical Report RSC-42, Remote Sensing Center, Texas A&M University, College Station, Texas, May 1973.

APPENDIX A

TABULATION OF EXPERIMENTAL DATA

The results of the airborne microwave radiometer experiment over selected test sites in Chickasha, Oklahoma are listed in Table A-I. The apparent temperatures for 5 data sets are provided according to Greenwich mean time and site designation.

Table A-II contains the listing of the data taken from the two passes made over the Weslaco flight line. The apparent temperatures for 5 data sets are provided according to Greenwich mean time.

Table A-III contains the results of the Chickasha ground measurements of soil moisture. The average soil moisture for both the North and South sampling lines is given with the standard deviation, σ , for each site. Table A-IV contains the vegetation moisture contents determined by taking sample cuttings of the wheat ground cover on the fields indicated.

TABLE A-1
 CHICKASHA APPARENT TEMPERATURES
 61.5 METERS - MARCH 14, 1972

HR	MIN	SEC	FIELD	1.42 GHZ		19.4 GHZ		37.0 GHZ	
				VERTICAL	HORIZONTAL	HORIZONTAL	HORIZONTAL	VERTICAL	HORIZONTAL
18	43	15.0	K	282.4	272.1	296.0	296.4	296.4	298.4
18	43	16.0	K	274.6	266.7	295.0	290.4	290.4	297.4
18	43	17.0	K	279.4	260.2	290.0	278.7	278.7	284.1
18	43	18.0	K	279.9	266.2	291.0	284.6	284.6	292.6
18	43	19.0	K	275.0	278.7	292.0	292.7	292.7	298.5
18	43	20.0	K	279.3	267.2	289.0	291.1	291.1	294.6
18	43	21.0	K	281.4	274.4	298.0	294.4	294.4	298.9
18	43	22.0	K	275.2	265.6	293.0	292.0	292.0	297.3
18	43	23.0	K	277.7	268.4	288.0	291.5	291.5	298.0
18	43	38.0	J	280.8	263.5	302.0	297.2	297.2	300.1
18	43	39.0	J	282.6	279.6	297.0	295.0	295.0	301.1
18	43	40.0	J	282.4	275.3	296.0	291.8	291.8	297.1
18	43	41.0	J	279.8	266.2	294.0	295.3	295.3	295.7
18	43	42.0	J	279.9	274.7	293.0	303.4	303.4	303.5
18	43	43.0	J	280.2	280.1	296.0	295.5	295.5	300.3
18	43	44.0	J	284.2	273.5	297.0	298.3	298.3	304.2
18	43	45.0	J	281.3	279.0	293.0	300.0	300.0	305.4
18	44	5.0	I	282.6	273.1	288.0	304.1	304.1	302.1
18	44	6.0	I	285.6	271.9	295.0	297.8	297.8	303.9
18	44	7.0	I	288.6	264.0	296.0	298.4	298.4	299.6
18	44	8.0	I	289.0	269.7	293.0	300.5	300.5	301.8
18	44	9.0	I	278.1	268.9	293.0	300.1	300.1	299.7
18	44	10.0	I	282.0	270.3	299.0	301.0	301.0	305.8
18	44	11.0	I	279.0	269.5	296.0	297.5	297.5	301.7

CONTINUATION OF TABLE A-1
 CHICKASPA APPARENT TEMPERATURES
 615 METERS - MARCH 14, 1972

HR	MIN	SEC	FIELD	1.42 GHZ		19.4 GHZ		37.0 GHZ	
				VERTICAL	HORIZONTAL	HORIZONTAL	HORIZONTAL	VERTICAL	HORIZONTAL
18	44	12.0	I	278.9	271.6	295.0	299.6	304.1	
18	44	13.0	I	282.6	269.6	296.0	300.9	304.9	
18	44	14.0	I	278.0	274.2	292.0	300.4	306.2	
18	44	15.0	I	289.2	269.3	292.0	299.7	302.3	
18	44	16.0	I	274.8	275.7	291.0	301.1	304.2	
18	44	17.0	I	289.4	274.3	294.0	297.3	301.0	
18	44	18.0	I	282.0	272.2	289.0	299.9	298.6	
18	44	19.0	I	271.3	264.8	294.0	301.4	304.5	
18	44	20.0	I	273.9	259.1	292.0	296.1	299.5	
18	44	21.0	I	275.4	271.1	292.0	299.1	303.1	
18	44	51.0	G	278.7	259.8	287.0	294.3	297.2	
18	44	52.0	G	285.3	267.6	291.0	291.6	296.4	
18	44	53.0	G	279.1	267.7	294.0	293.8	295.9	
18	44	54.0	G	280.1	261.7	290.0	294.4	296.6	
18	44	55.0	G	271.7	264.6	290.0	295.8	301.3	
18	44	56.0	G	267.1	259.9	295.0	298.7	299.3	
18	54	24.0	H	278.2	274.6	292.0	296.1	293.3	
18	54	25.0	H	280.1	272.6	288.0	293.5	294.9	
18	54	49.0	G	279.3	276.4	291.0	295.5	297.5	
18	54	50.0	G	281.2	277.6	293.0	294.7	299.8	
18	54	51.0	G	277.1	276.8	292.0	304.0	307.2	
18	54	52.0	G	279.2	267.7	293.0	302.3	306.1	
18	54	53.0	G	278.2	271.1	290.0	293.6	299.5	
18	55	9.0	F	278.4	277.0	291.0	297.6	305.3	

CONTINUATION OF TABLE A-I
 CHICKASHA APPARENT TEMPERATURES
 615 METERS - MARCH 14, 1972

TIME HR MIN SEC	FIELD	1.42 GHZ		19.4 GHZ		37.0 GHZ	
		VERTICAL	HORIZONTAL	HORIZONTAL	VERTICAL	HORIZONTAL	VERTICAL
18 55 10.0	F	292.9	274.4	295.0	295.8	300.3	
18 55 11.0	F	282.2	276.8	289.0	298.4	300.9	
18 55 12.0	F	280.0	274.7	291.0	303.0	304.4	
18 55 13.0	F	273.5	263.1	284.0	291.3	297.6	
18 55 14.0	F	279.1	264.4	289.0	294.3	299.3	
18 55 15.0	F	273.2	262.7	284.0	293.3	301.7	
18 55 22.0	E	277.7	266.3	292.0	297.9	302.6	
18 55 23.0	E	271.4	263.7	284.0	294.8	299.8	
18 55 24.0	E	271.4	256.7	286.0	287.8	299.2	
18 55 25.0	E	262.0	254.4	277.0	270.0	285.7	
18 55 26.0	E	264.5	250.5	286.0	288.4	290.6	
18 56 26.0	D	285.8	275.4	294.0	301.0	302.7	
18 56 27.0	D	281.9	275.5	298.0	300.7	300.8	
18 56 28.0	D	282.4	269.4	295.0	294.4	296.9	
18 56 29.0	D	273.9	269.4	288.0	298.4	304.6	
18 56 30.0	D	284.0	267.0	288.0	301.0	305.1	
18 56 31.0	D	273.4	261.4	288.0	297.5	299.9	
18 56 54.0	C	285.1	272.6	290.0	297.2	302.4	
18 56 55.0	C	239.9	274.3	290.0	297.6	302.4	
18 56 56.0	C	282.4	271.5	290.0	299.0	302.0	
18 56 57.0	C	270.9	263.6	294.0	296.1	298.0	
18 56 58.0	C	261.8	241.5	292.0	295.7	300.8	
18 57 34.0	B	279.8	271.7	287.0	298.1	303.9	
18 57 35.0	B	276.6	265.0	291.0	292.5	302.0	

CONTINUATION OF TABLE A-1
 CHICKASHA APPARENT TEMPERATURES
 615 METERS - MARCH 14, 1972

HR	MIN	SEC	FIELD	1.42 GHZ		1.42 GHZ		19.4 GHZ		37.0 GHZ	
				VERTICAL	HORIZONTAL	VERTICAL	HORIZONTAL	VERTICAL	HORIZONTAL		
18	57	36.0	B	273.8	263.1	293.0	299.0	301.2			37.0 GHZ HORIZONTAL
18	57	37.0	B	270.1	253.6	291.0	305.2	308.9			
18	58	11.0	A	278.8	274.8	287.0	294.2	300.3			
18	58	12.0	A	279.3	264.9	294.0	297.2	298.1			
18	58	13.0	A	264.9	256.8	292.0	298.0	305.5			
19	5	51.0	K	277.9	272.8	295.0	299.1	298.1			
19	5	52.0	K	283.2	271.8	289.0	297.2	297.9			
19	5	53.0	K	285.2	270.2	297.0	293.8	299.2			
19	5	54.0	K	278.1	270.3	287.0	296.1	302.3			
19	5	55.0	K	285.3	280.7	294.0	294.6	296.9			
19	5	56.0	K	284.2	270.0	291.0	294.0	294.8			
19	5	57.0	K	285.5	275.3	290.0	298.9	304.0			
19	5	58.0	K	279.3	267.7	292.0	304.7	304.9			
19	6	14.0	J	286.4	274.2	300.0	298.1	304.5			
19	6	15.0	J	282.5	276.5	296.0	301.6	308.2			
19	6	16.0	J	283.5	277.5	292.0	299.2	306.3			
19	6	17.0	J	277.9	273.5	289.0	302.2	306.7			
19	6	18.0	J	282.4	275.0	291.0	304.1	309.8			
19	6	19.0	J	286.4	271.2	294.0	294.7	300.1			
19	6	20.0	J	288.0	280.4	296.0	298.7	303.7			
19	6	36.0	I	279.7	271.9	295.0	301.9	306.2			
19	6	37.0	I	275.6	272.0	294.0	296.5	301.3			
19	6	38.0	I	286.2	277.4	292.0	301.2	303.4			
19	6	39.0	I	281.1	267.9	297.0	298.2	299.6			

CONTINUATION OF TABLE A-I
 CHICKASHA APPARENT TEMPERATURES
 615 METERS - MARCH 14, 1972

HR	MIN	SEC	FIELD	1.42 GHZ		19.4 GHZ		37.0 GHZ	
				VERTICAL	HORIZONTAL	HORIZONTAL	VERTICAL	VERTICAL	HORIZONTAL
19	6	40.0	I	284.8	267.2	299.0	300.6	306.0	306.0
19	6	41.0	I	286.4	273.8	292.0	300.4	305.0	305.0
19	6	42.0	I	280.3	272.2	288.0	295.9	299.6	299.6
19	6	43.0	I	290.4	281.7	296.0	300.5	305.4	305.4
19	6	44.0	I	281.9	278.3	294.0	300.4	305.2	305.2
19	6	45.0	I	290.0	280.0	292.0	298.8	304.7	304.7
19	6	46.0	I	288.2	276.2	299.0	301.4	307.1	307.1
19	6	47.0	I	290.1	279.8	300.0	301.6	306.3	306.3
19	6	48.0	I	286.3	276.9	288.0	303.3	306.0	306.0
19	6	49.0	I	283.0	273.5	291.0	305.7	306.6	306.6
19	6	50.0	I	273.5	264.6	295.0	300.9	305.7	305.7
19	7	21.0	G	280.9	269.3	293.0	302.0	304.0	304.0
19	7	22.0	G	282.6	274.9	298.0	301.9	304.9	304.9
19	7	23.0	G	279.1	266.0	297.0	302.7	303.7	303.7
19	7	24.0	G	274.4	267.8	286.0	296.7	303.1	303.1
19	7	25.0	G	272.2	259.0	291.0	300.4	303.3	303.3
19	21	13.0	B	273.4	270.1	293.0	295.3	303.8	303.8
19	21	14.0	B	279.6	267.9	291.0	292.7	302.7	302.7
19	21	15.0	B	278.0	273.0	294.0	298.5	303.2	303.2
19	21	16.0	B	274.6	267.4	290.0	300.6	306.7	306.7
19	21	50.0	A	272.4	262.2	292.0	295.5	302.9	302.9
19	21	51.0	A	273.8	264.4	291.0	302.5	304.9	304.9
19	21	52.0	A	259.9	249.0	288.0	296.9	303.0	303.0

TABLE A-II

WESLACO APPARENT TEMPERATURES
615 METERS - MARCH 14, 1972

HR	MIN	SEC	FIELD	1.42 GHZ		19.4 GHZ		37.0 GHZ	
				VERTICAL	HORIZONTAL	HORIZONTAL	HORIZONTAL	VERTICAL	HORIZONTAL
21	14	44.0		210.2	192.5	222.0	240.9	259.3	
21	14	44.5		212.0	201.4	222.0	228.6	255.3	
21	14	45.0		220.2	211.1	240.0	234.8	261.2	
21	14	45.5		234.0	218.8	240.0	240.1	264.2	
21	14	46.0		234.6	227.7	253.0	267.2	277.3	
21	14	46.5		234.7	226.7	253.0	278.9	284.6	
21	14	47.0		221.5	211.7	210.0	282.4	287.0	
21	14	47.5		210.1	206.2	210.0	271.8	279.3	
21	14	48.0		207.0	190.5	180.0	243.7	258.8	
21	14	48.5		198.5	182.2	180.0	234.7	253.5	
21	14	49.0		193.0	177.4	194.0	221.7	244.5	
21	14	49.5		197.9	174.9	194.0	202.0	234.3	
21	14	50.0		183.2	165.7	184.0	197.3	226.2	
21	14	50.5		190.9	158.7	184.0	214.3	239.8	
21	14	51.0		188.1	162.4	200.0	212.8	241.3	
21	14	51.5		190.3	172.3	200.0	220.9	245.0	
21	14	52.0		183.9	175.9	203.0	221.1	252.2	
21	14	52.5		184.0	167.5	203.0	220.7	248.2	
21	14	53.0		190.1	170.8	217.0	226.2	251.6	
21	14	53.5		185.4	172.0	217.0	222.4	255.7	
21	14	54.0		182.5	173.2	200.0	231.0	253.5	
21	14	54.5		187.0	175.3	200.0	233.6	260.2	
21	14	55.0		191.4	172.1	215.0	225.1	260.3	
21	14	55.5		190.4	172.1	215.0	229.2	257.2	

CONTINUATION OF TABLE A-II
 WESLACO APPARENT TEMPERATURES
 615 METERS - MARCH 14, 1972

TIME HR MIN SEC	FIELD	1.42 GHZ		1.42 GHZ		19.4 GHZ		37.0 GHZ	
		VERTICAL	HORIZONTAL	VERTICAL	HORIZONTAL	VERTICAL	HORIZONTAL	VERTICAL	HORIZONTAL
21 14 56.0		192.8	176.2	178.4	212.0	237.8	258.2	230.5	258.9
21 14 56.5		184.0	170.2	186.4	212.0	226.5	247.9	235.4	260.0
21 14 57.0		193.4	175.0	188.6	216.0	229.8	254.3	226.7	248.3
21 14 57.5		201.4	179.3	205.9	216.0	232.9	257.9	221.1	245.7
21 14 58.0		198.9	180.0	232.0	220.0	243.7	264.2	223.1	246.7
21 14 58.5		199.9	178.4	241.7	220.0	252.4	269.3	237.8	258.2
21 14 59.0		206.0	186.4	257.3	223.0	262.4	272.1	226.5	247.9
21 14 59.5		213.2	188.6	258.6	223.0	272.5	275.3	229.8	254.3
21 15 -0.0		212.9	205.9	251.4	245.0	265.2	273.9	232.9	257.9
21 15 0.5		230.0	232.0	249.7	245.0	274.9	282.2	243.7	264.2
21 15 1.0		248.1	241.7	244.6	237.0	282.1	287.4	252.4	269.3
21 15 1.5		258.9	257.3	231.9	237.0	274.7	285.2	262.4	272.1
21 15 2.0		267.5	258.6	227.7	257.0	274.7	285.2	272.5	275.3
21 15 2.5		264.9	251.4	227.7	257.0	274.9	282.2	265.2	273.9
21 15 3.0		256.4	249.7	244.6	263.0	282.1	287.4	274.9	282.2
21 15 3.5		248.9	244.6	231.9	263.0	274.7	285.2	282.1	287.4
21 15 4.0		240.4	231.9	227.7	260.0	274.7	285.2	274.7	285.2
21 15 4.5		248.1	227.7	234.1	260.0	274.0	284.4	274.0	284.4
21 15 5.0		243.9	234.1	216.6	241.0	280.1	281.3	280.1	281.3
21 15 5.5		240.8	216.6	218.3	241.0	275.8	287.6	275.8	287.6
21 15 6.0		228.9	218.3	196.1	208.0	274.9	279.9	274.9	279.9
21 15 6.5		207.0	196.1	189.6	208.0	263.0	273.7	263.0	273.7
21 15 7.0		202.9	189.6	185.1	207.0	235.6	254.1	235.6	254.1
21 15 7.5		200.3	185.1		207.0	222.8	245.4	222.8	245.4

CONTINUATION OF TABLE A-II
 WESLACO APPARENT TEMPERATURES
 615 METERS - MARCH 14, 1972

TIME HR MIN SEC	FIELD	1.42 GHZ		19.4 GHZ		37.0 GHZ	
		VERTICAL	HORIZONTAL	HORIZONTAL	VERTICAL	VERTICAL	HORIZONTAL
21 15 8.0		197.7	189.4	210.0	215.0	240.9	
21 15 8.5		206.4	206.1	210.0	226.4	253.4	
21 15 9.0		202.1	194.4	211.0	231.9	256.3	
21 15 9.5		208.0	193.3	211.0	232.6	257.5	
21 15 10.0		208.8	194.0	238.0	231.8	254.2	
21 15 10.5		212.1	209.5	238.0	226.4	255.4	
21 15 11.0		227.2	219.7	234.0	230.1	257.2	
21 15 11.5		236.3	233.4	234.0	255.0	269.8	
21 15 12.0		223.4	213.4	204.0	263.1	274.1	
21 15 12.5		193.9	191.0	204.0	254.0	267.7	
21 15 13.0		197.6	186.6	207.0	237.9	259.6	
21 15 13.5		202.5	193.6	207.0	228.5	255.6	
21 15 14.0		205.4	193.5	234.0	230.5	253.7	
21 15 14.5		223.5	220.9	234.0	236.6	264.0	
21 15 15.0		235.1	237.0	246.0	238.5	261.8	
21 15 15.5		252.4	255.3	246.0	267.9	280.1	
21 15 16.0		258.9	263.2	261.0	273.8	277.2	
21 15 16.5		266.4	256.4	261.0	278.6	285.3	
21 15 17.0		262.4	258.9	258.0	271.5	277.0	
21 15 17.5		256.6	245.9	258.0	277.2	280.4	
21 15 18.0		245.7	240.9	209.0	280.4	280.0	
21 15 18.5		229.5	232.1	209.0	274.4	277.2	
21 15 19.0		222.3	221.6	222.0	254.8	270.6	
21 15 19.5		229.3	225.0	222.0	245.8	262.6	

CONTINUATION OF TABLE A-II
 WESLACO APPARENT TEMPERATURES
 615 METERS - MARCH 14, 1972

HR	TIME MIN SEC	FIELD	1.42 GHZ		19.4 GHZ		37.0 GHZ	
			VERTICAL	HORIZONTAL	HORIZONTAL	HORIZONTAL	VERTICAL	HORIZONTAL
21	15	20.0	219.8	216.9	227.0	252.5	265.7	
21	15	20.5	223.7	217.7	227.0	249.3	256.4	
21	15	21.0	223.4	217.9	264.0	252.4	266.2	
21	15	21.5	223.2	229.2	264.0	251.4	267.9	
21	15	22.0	223.4	221.1	256.0	262.8	278.2	
21	15	22.5	235.8	226.9	266.0	267.8	281.6	
21	15	23.0	245.8	238.5	278.0	269.4	279.0	
21	15	23.5	241.4	245.6	278.0	274.7	285.2	
21	15	24.0	251.1	243.4	262.0	283.2	291.9	
21	15	24.5	238.2	226.2	262.0	289.4	298.7	
21	24	39.0	229.7	197.8	195.0	272.3	280.6	
21	24	39.5	210.8	193.6	195.0	267.7	276.4	
21	24	40.0	210.6	187.1	253.0	249.5	258.4	
21	24	40.5	222.0	202.7	253.0	234.2	257.2	
21	24	41.0	227.2	216.4	241.0	232.9	255.6	
21	24	41.5	232.9	225.7	241.0	239.8	264.0	
21	24	42.0	237.9	228.9	262.0	244.5	267.5	
21	24	42.5	227.3	220.9	262.0	259.6	270.6	
21	24	43.0	225.6	215.0	206.0	272.0	279.5	
21	24	43.5	209.9	194.6	206.0	271.7	281.8	
21	24	44.0	197.6	191.8	209.0	260.4	280.0	
21	24	44.5	195.5	181.9	209.0	240.4	258.6	
21	24	45.0	200.7	164.0	186.0	240.4	250.7	
21	24	45.5	183.2	153.1	186.0	234.8	257.1	

CONTINUATION OF TABLE A-II
 WESLACO APPARENT TEMPERATURES
 615 METERS - MARCH 14, 1972

HR	MIN	SEC	FIELD		1.42 GHZ		19.4 GHZ		37.0 GHZ	
			VERTICAL	HORIZONTAL	VERTICAL	HORIZONTAL	VERTICAL	HORIZONTAL		
21	24	46.0	187.3	167.1	198.0	225.1	245.1			
21	24	46.5	185.1	161.9	198.0	214.0	241.8			
21	24	47.0	187.5	162.9	198.0	215.9	244.9			
21	24	47.5	188.2	172.1	198.0	227.7	247.8			
21	24	48.0	189.9	170.5	213.0	225.7	251.8			
21	24	48.5	199.1	166.4	213.0	230.0	257.5			
21	24	49.0	187.5	166.4	195.0	229.5	253.7			
21	24	49.5	186.1	164.4	195.0	228.3	257.6			
21	24	50.0	183.4	161.3	211.0	229.9	256.1			
21	24	50.5	185.8	164.4	211.0	229.5	258.3			
21	24	51.0	191.0	171.8	211.0	233.4	259.9			
21	24	51.5	190.0	175.0	211.0	233.9	259.7			
21	24	52.0	188.2	178.6	236.0	230.2	257.1			
21	24	52.5	193.6	173.5	236.0	231.7	257.5			
21	24	53.0	197.4	178.2	196.0	232.8	259.1			
21	24	53.5	198.9	174.3	196.0	236.7	253.1			
21	24	54.0	193.0	175.6	208.0	237.9	261.6			
21	24	54.5	204.1	177.5	208.0	226.6	253.7			
21	24	55.0	205.8	182.8	209.0	216.6	235.8			
21	24	55.5	205.9	191.1	209.0	222.7	249.2			
21	24	56.0	205.6	185.4	208.0	240.8	264.7			
21	24	56.5	204.7	185.5	208.0	241.9	259.0			
21	24	57.0	203.7	200.3	239.0	235.5	258.6			
21	24	57.5	218.0	208.5	239.0	239.9	259.1			

CONTINUATION OF TABLE A-II
 WESLACO APPARENT TEMPERATURES
 615 METERS - MARCH 14, 1972

TIME HR MIN SEC	FIELD	1.42 GHZ		19.4 GHZ		37.0 GHZ	
		VERTICAL	HORIZONTAL	VERTICAL	HORIZONTAL	VERTICAL	HORIZONTAL
21 24 58.0		233.6	227.1	230.0	240.5	263.7	
21 24 58.5		247.7	240.9	230.0	249.8	268.5	
21 24 59.0		257.8	253.4	240.0	257.3	272.2	
21 24 59.5		266.4	260.0	240.0	267.2	272.1	
21 25 -0.0		262.0	252.6	256.0	269.0	270.7	
21 25 0.5		264.7	255.2	256.0	270.9	276.3	
21 25 1.0		263.9	254.1	261.0	276.6	286.4	
21 25 1.5		259.6	259.8	261.0	279.6	286.4	
21 25 2.0		263.6	266.9	264.0	281.4	288.2	
21 25 2.5		258.1	254.3	264.0	279.3	288.1	
21 25 3.0		263.7	262.1	259.0	285.7	289.4	
21 25 3.5		258.0	252.0	259.0	287.0	288.0	
21 25 4.0		244.6	239.8	198.0	285.0	284.3	
21 25 4.5		231.9	219.7	198.0	285.4	286.1	
21 25 5.0		212.8	199.8	205.0	274.9	282.6	
21 25 5.5		213.9	191.7	205.0	259.5	276.5	
21 25 6.0		212.1	199.1	232.0	227.9	256.9	
21 25 6.5		216.9	196.2	232.0	225.8	251.3	
21 25 7.0		220.2	200.6	211.0	216.7	249.1	
21 25 7.5		215.2	198.3	211.0	232.8	260.1	
21 25 8.0		207.3	191.2	203.0	239.1	267.2	
21 25 8.5		209.4	196.9	203.0	232.5	255.3	
21 25 9.0		219.2	209.8	244.0	231.7	258.4	
21 25 9.5		234.4	215.4	244.0	230.6	259.6	

CONTINUATION OF TABLE A-II
 WFLACO APPARENT TEMPERATURES
 615 METERS - MARCH 14, 1972

TIME HR MIN SEC	FIELD	1.42 GHZ		19.4 GHZ		37.0 GHZ	
		VERTICAL	HORIZONTAL	HORIZONTAL	HORIZONTAL	VERTICAL	HORIZONTAL
21 25 10.0		229.8	222.8	246.0	223.3	252.2	252.2
21 25 10.5		227.5	219.4	246.0	243.9	262.0	262.0
21 25 11.0		214.1	201.1	199.0	258.7	269.3	269.3
21 25 11.5		210.5	190.2	199.0	264.4	279.1	279.1
21 25 12.0		199.4	181.8	206.0	248.7	268.6	268.6
21 25 12.5		193.7	182.4	206.0	225.8	253.7	253.7
21 25 13.0		202.7	195.5	234.0	227.6	255.2	255.2
21 25 13.5		214.8	215.2	234.0	229.8	260.9	260.9
21 25 14.0		231.4	229.7	251.0	238.9	265.3	265.3
21 25 14.5		239.0	246.7	251.0	250.6	263.0	263.0
21 25 15.0		254.8	252.9	274.0	265.0	277.5	277.5
21 25 15.5		255.2	248.8	274.0	271.8	278.8	278.8
21 25 16.0		254.3	262.2	213.0	272.3	279.1	279.1
21 25 16.5		250.1	250.9	213.0	281.8	290.3	290.3
21 25 17.0		252.1	239.5	217.0	282.6	285.6	285.6
21 25 17.5		239.3	230.0	217.0	273.1	283.4	283.4
21 25 18.0		227.7	224.2	198.0	282.3	282.1	282.1
21 25 18.5		222.9	223.3	198.0	276.9	279.1	279.1
21 25 19.0		210.9	214.3	232.0	258.6	269.2	269.2
21 25 19.5		215.1	219.1	232.0	250.0	265.8	265.8
21 25 20.0		214.2	214.1	236.0	247.9	264.1	264.1
21 25 20.5		214.8	209.9	236.0	247.5	260.7	260.7
21 25 21.0		218.2	216.2	238.0	255.9	267.1	267.1
21 25 21.5		229.9	222.3	238.0	258.6	269.6	269.6

CONTINUATION OF TABLE A-II
 WESLACO APPARENT TEMPERATURES
 615 METERS - MARCH 14, 1972

TIME HR MIN SEC	FIELD	1.42 GHZ		1.42 GHZ		19.4 GHZ		37.0 GHZ	
		VERTICAL	HORIZONTAL	VERTICAL	HORIZONTAL	VERTICAL	HORIZONTAL	VERTICAL	HORIZONTAL
21 25 22.0		227.5	226.2	249.7	250.0	271.0	272.5	280.2	284.7
21 25 22.5		233.6	243.6	241.8	196.0	196.0	270.8	270.8	282.9
21 25 23.0		246.4	249.7	236.9	271.0	271.0	280.9	280.9	288.2
21 25 23.5		250.7	228.2	229.5	250.0	250.0	286.3	286.3	294.2
21 25 24.0		240.5	186.5	200.2	195.0	195.0	292.4	292.4	298.4
21 25 24.5		229.5	180.5	202.2	195.0	195.0	231.4	231.4	257.3
21 25 44.0		197.3	176.7	197.3	197.0	197.0	231.0	231.0	256.0
21 25 44.5		198.0	184.1	198.0	197.0	197.0	226.7	226.7	251.1
21 25 45.5		207.0	178.3	207.0	199.0	199.0	227.4	227.4	255.8
21 25 46.0		196.2	183.7	196.2	199.0	199.0	225.9	225.9	258.7
21 25 46.5		199.8	188.7	199.8	213.0	213.0	228.6	228.6	255.5
21 25 47.0		201.9	198.4	201.9	213.0	213.0	223.6	223.6	257.3
21 25 47.5		215.1	205.1	215.1	206.0	206.0	224.1	224.1	259.1
21 25 48.0		221.8	212.1	221.8	206.0	206.0	232.5	232.5	260.9
21 25 48.5		217.6	197.7	217.6	206.0	206.0	235.1	235.1	261.0
21 25 49.0		224.1	202.3	224.1	249.0	249.0	251.5	251.5	270.9
21 25 49.5		216.7	199.6	216.7	249.0	249.0	253.1	253.1	273.1
21 25 50.0		216.4	191.5	216.4	235.0	235.0	244.5	244.5	269.3
21 25 50.5		227.8	204.0	227.8	235.0	235.0	262.5	262.5	276.6
21 25 51.0		227.4	210.0	227.4	259.0	259.0	265.5	265.5	274.3
21 25 51.5		234.6	216.0	234.6	259.0	259.0	255.6	255.6	273.1
21 25 52.0		235.7	216.0	235.7	271.0	271.0	249.7	249.7	271.9
21 25 52.5			207.2		271.0	271.0	273.6	273.6	283.6

CONTINUATION OF TABLE A-II
 WESLACO APPARENT TEMPERATURES
 615 METERS - MARCH 14, 1972

HR	TIME MIN SEC	FIELD	1.42 GHZ		19.4 GHZ		37.0 GHZ	
			VERTICAL	HORIZONTAL	HORIZONTAL	HORIZONTAL	VERTICAL	HORIZONTAL
21	25	53.0	224.2	206.1	268.0	289.5	293.7	
21	25	53.5	222.6	201.4	268.0	283.8	288.9	
21	25	54.0	226.3	203.8	265.0	289.8	293.5	
21	25	54.5	221.3	198.2	265.0	281.4	292.6	
21	25	55.0	226.4	207.3	218.0	285.3	299.1	
21	25	55.5	219.2	210.8	218.0	289.8	297.1	
21	25	56.0	212.9	210.7	218.0	275.3	287.5	
21	25	56.5	213.7	206.3	218.0	246.7	266.5	
21	25	57.0	215.7	196.9	218.0	240.5	262.3	
21	25	57.5	221.7	201.9	218.0	240.9	256.2	
21	25	58.0	221.0	217.2	232.0	241.9	256.7	
21	25	58.5	231.4	228.2	232.0	234.3	251.9	
21	25	59.0	248.7	238.9	242.0	235.0	254.2	
21	25	59.5	248.5	247.0	242.0	246.4	259.2	
21	26	-0.0	261.1	251.1	237.0	264.1	266.9	
21	26	0.5	250.3	248.0	237.0	271.8	277.3	
21	26	1.0	258.6	232.0	235.0	271.1	277.8	
21	26	1.5	247.8	230.2	235.0	264.9	270.9	
21	26	2.0	219.9	205.7	206.0	259.5	266.9	
21	26	2.5	202.6	189.6	206.0	255.2	266.2	
21	26	3.0	194.7	185.9	210.0	246.3	260.9	
21	26	3.5	199.1	188.2	210.0	243.6	259.5	
21	26	4.0	197.9	188.6	212.0	234.7	261.2	
21	26	4.5	201.4	189.4	212.0	226.0	252.4	

CONTINUATION OF TABLE A-II
 WESLACO APPARENT TEMPERATURES
 615 METERS - MARCH 14, 1972

HR	MIN	SEC	FIELD	1.42 GHZ		19.4 GHZ		37.0 GHZ	
				VERTICAL	HORIZONTAL	HORIZONTAL	VERTICAL	VERTICAL	HORIZONTAL
21	26	5.0		205.7	187.9	198.0	234.3	256.8	
21	26	5.5		201.4	184.3	198.0	236.4	259.3	
21	26	6.0		197.7	190.6	195.0	235.5	258.2	
21	26	6.5		205.2	198.8	195.0	225.5	251.2	
21	26	7.0		219.6	220.8	256.0	213.0	246.6	
21	26	7.5		233.9	233.1	256.0	218.5	250.5	
21	26	8.0		235.4	244.9	254.0	237.0	265.2	
21	26	8.5		241.0	247.1	254.0	278.1	290.8	
21	26	9.0		238.0	239.9	250.0	278.8	285.7	
21	26	9.5		242.6	236.0	250.0	280.8	286.4	
21	26	10.0		236.8	243.3	242.0	287.3	286.9	
21	26	10.5		239.2	243.8	242.0	278.1	285.3	
21	26	11.0		242.9	243.5	248.0	283.1	283.7	
21	26	11.5		225.4	234.9	248.0	282.2	285.6	
21	26	12.0		238.4	241.3	252.0	272.6	277.1	
21	26	12.5		242.3	249.5	252.0	276.7	281.9	
21	26	13.0		249.4	249.9	255.0	278.0	285.8	
21	26	13.5		240.4	235.6	255.0	287.7	292.3	
21	26	14.0		235.1	224.8	209.0	289.3	290.5	
21	26	14.5		237.9	216.0	209.0	284.1	293.0	
21	26	15.0		226.0	210.4	229.0	262.9	276.8	
21	26	15.5		220.2	216.7	229.0	246.7	265.8	
21	26	16.0		215.7	216.5	235.0	246.2	272.3	
21	26	16.5		225.9	229.6	235.0	243.8	266.7	

CONTINUATION OF TABLE A-II
 WESLACO APPARENT TEMPERATURES
 615 METERS - MARCH 14, 1972

TIME		FIELD	1.42 GHZ		19.4 GHZ		37.0 GHZ	
HR	MIN SEC		VERTICAL	HORIZONTAL	HORIZONTAL	VERTICAL	VERTICAL	HORIZONTAL
21	26	17.0	221.6	219.0	225.0	246.6	265.8	
21	26	17.5	222.8	215.3	225.0	253.6	273.7	
21	26	18.0	220.2	205.0	213.0	255.8	271.7	
21	26	18.5	208.0	193.9	213.0	251.2	274.2	
21	26	19.0	223.6	210.4	207.0	237.2	262.4	
21	26	19.5	226.9	208.4	207.0	239.5	263.8	
21	26	20.0	230.1	217.3	254.0	240.2	264.3	
21	26	20.5	241.5	233.0	254.0	251.4	269.0	
21	26	21.0	232.9	231.7	249.0	270.9	284.2	
21	26	21.5	247.8	235.5	249.0	280.2	292.2	
21	26	22.0	254.5	251.8	249.0	268.6	286.5	
21	26	22.5	254.8	253.3	249.0	269.9	278.5	
21	26	23.0	263.8	254.0	251.0	276.3	279.8	
21	26	23.5	250.9	251.5	251.0	281.0	281.5	
21	26	24.0	236.8	230.1	210.0	281.4	283.0	
21	26	24.5	224.7	213.7	210.0	279.4	283.8	

Table A-III
Soil Moisture Summary
Chickasha Sites

<u>Site</u>	Average Soil Moisture Content			
	<u>North Line</u>	<u>σ</u>	<u>South Line</u>	<u>σ</u>
A	5.52	1.11	7.22	3.01
B	7.31	1.25	7.99	1.69
C	7.53	0.65	7.89	1.32
D	8.04	1.17	8.72	1.33
E	8.83	1.75	9.52	2.31
F	11.38	2.03	11.94	3.23
G	4.92	0.48	5.66	1.89
H	14.20	3.12	13.08	3.69
I	7.53	1.66	8.45	1.73
J	10.28	2.09	12.14	2.72
K	8.31	1.93	9.83	0.79

Table A-IV
Wheat Samples from Chickasha Sites

<u>Site</u>	<u>Percent Moisture (Dry Weight Basis)</u>
A	285.00 163.81
B	Insufficient wheat for cutting sample
C	245.87
D	183.65
E	51.53 119.38
F	134.22
G	233.05
H	375.30
I	208.06 200.96
J	262.82
K	230.57 320.47

The REMOTE SENSING CENTER was established by authority of the Board of Directors of the Texas A&M University System on February 27, 1968. The CENTER is a consortium of four colleges of the University; Agriculture, Engineering, Geosciences, and Science. This unique organization concentrates on the development and utilization of remote sensing techniques and technology for a broad range of applications to the betterment of mankind.

